1   **Bond type and discretization of non-muscle myosin II are critical for simulated**
2   **contractile dynamics**

3

4   D.B Cortes, M. Gordon, F. Nédélec, A.S. Maddox

5

6   Running Head: Tuning motor bonding and coarse-graining

ABSTRACT

Molecular motors drive cytoskeletal rearrangements to change cell shape. Myosins are the motors that move, crosslink, and modify the actin cytoskeleton. The primary force generator in contractile actomyosin networks is non-muscle myosin II (NMMII), a molecular motor that assembles into ensembles that bind, slide, and crosslink actin filaments (F-actin). The multivalence of NMMII ensembles and their multiple roles have confounded the resolution of crucial questions including how the number of NMMII subunits affects dynamics, and what affects the relative contribution of ensembles' crosslinking versus motoring activities. Since biophysical measurements of ensembles are sparse, modeling of actomyosin networks has aided in discovering the complex behaviors of NMMII ensembles. Myosin ensembles have been modeled via several strategies with variable discretization/coarse-graining and unbinding dynamics, and while general assumptions that simplify motor ensembles result in global contractile behaviors, it remains unclear which strategies most accurately depict cellular activity. Here, we used an agent-based platform, Cytosim, to implement several models of NMMII ensembles. Comparing the effects of bond type, we found that ensembles of catch-slip and catch motors were the best force generators and binders of filaments. Slip motor ensembles were capable of generating force but unbound frequently, resulting in slower contractile rates of contractile networks. Coarse-graining of these ensemble types from two sets of 16 motors on opposite ends of a stiff rod to two binders, each representing 16 motors, reduced force generation, contractility, and the total connectivity of filament networks for all ensemble types. A parallel cluster model (PCM) previously used to describe ensemble dynamics via statistical mechanics, allowed better contractility with coarse-graining, though connectivity was still markedly reduced for this ensemble type with coarse-

1 graining. Together our results reveal substantial trade-offs associated with the process of

2 coarse-graining NMMII ensembles and highlight the robustness of discretized catch-slip

3 ensembles in modeling actomyosin networks.

4

5 **STATEMENT OF SIGNIFICANCE**

6 Agent-based simulations of contractile networks allow us to explore the mechanics

7 of actomyosin contractility, which drives many cell shape changes including cytokinesis,

8 the final step of cell division. Such simulations should be able to predict the mechanics

9 and dynamics of non-muscle contractility, however recent work has highlighted a lack of

10 consensus on how to best model the non-muscle myosin II. These ensembles of

11 approximately 32 motors are the key components responsible for driving contractility.

12 Here, we explored different methods for modeling non-muscle myosin II ensembles within

13 the context of contractile actomyosin networks. We show that the level of coarse-graining

14 and the choice of unbinding model used to model motor unbinding under load indeed has

15 profound effects on contractile network dynamics.

16

17 **INTRODUCTION**

18 Non-muscle myosin II (NMMII) is an actin-based motor that forms ensembles with

19 12-32 motor domain pairs extending from the ends of a rod formed by the bundled coiled-

20 coil tails of the NMMII heavy chains (1–3). NMMII drives a myriad of cellular and tissue-

21 level processes during cell migration, morphogenesis and cell division (4–7). Cytokinesis,

22 one of these processes, is the last stage of cell division, is the physical division of one

1   cell into two. Cytokinesis is powered by a cortical actomyosin band known as the

2   cytokinetic ring, which forms in anaphase and constricts to invaginate the plasma

3   membrane and partition the cytoplasm.

4   NMMII is capable of sliding actin filaments through its motoring activity (3, 8–11).

5   However, NMMII motor ensembles are also robust F-actin crosslinkers (1, 8, 9, 12). Thus,

6   it is unclear whether NMMII ensembles generate contractile forces through motor activity-

7   dependent polarity sorting of actin filaments, which would induce filament buckling in a

8   crosslinked network (13–16), or through passive crosslinking of depolymerizing or

9   treadmilling F-actin (17, 18). The former hypothesis predicts complete failure of

10   cytokinesis with motor-dead NMMII, while the latter predicts that motor activity is

11   dispensable. Work with mammalian cultured cells and the budding yeast, *S. cerevisiae,*

12   provided evidence for contractility with NMMII lacking the motor domain (17) or with

13   motor-deficient NMMII (19), suggesting that NMMII primarily contributes as a crosslinker.

14   However, work with similar NMMII mutants in *Drosophila* and *Caenorhabditis elegans*

15   concluded that NMMII motor activity is required for cytokinesis in embryonic cells and

16   tissues (20, 21). Separation of motor and crosslinking activities *in vivo* is confounded by

17   observations that some motor-dead isoforms bind F-actin more tightly or for longer than

18   wild-type NMMII and are thus crosslinking gain-of-function (20). Interestingly, contractile

19   speed is not a linear function of the abundances of both NMMII and non-motor

20   crosslinkers, as intermediate levels were observed to confer optimal contractile dynamics

21   (15, 22–24). Defining the relative contributions of NMMII motoring and crosslinking to

22   contractility is difficult, but nevertheless essential, since it will shed light on the mechanics

4

1   of non-muscle contractility in the context of cellular processes such as contractility, cell

2   motility and epithelial morphogenesis.

3   While biophysics, biochemistry and cell biology have revealed much about the

4   contributions of NMMII to non-muscle contractility, the complex behavior of NMMII

5   ensembles has remained hard to determine *in vivo.* A complementary approach can be

6   found in agent-based modeling, wherein collective behaviors emerge from the explicit

7   simulation of the components and their interactions. For this purpose, several open-

8   source modeling suites that specialize in cytoskeletal dynamics are available (25–28).

9   However, herein the question of how to best model ensembles of motors arises.

10   Interestingly, the best method to model motor ensembles is unresolved. Even for single

11   NMMII motors, unbinding dynamics under force is unknown. Generally, non-covalent

12   bonds are described as slip bonds, where bond lifetime decays exponentially with

13   increasing applied load (Fig. 1A). Some molecular motors, like dynein and kinesins, fall

14   into this regime (29, 30); *in silico* unbinding dynamics akin to slip bonds can be modeled

15   by use of Kramers' theory or Bell's Law (31). By contrast, some myosin motors or

16   collections of myosin motors exhibit emergent catch-bond dynamics (32), behavior that

17   can be modeled *in silico* by considering collections of motors (33, 34). Catch bond

18   dynamics can be described generally by an exponential increase in bond lifetime as force

19   is applied up to a critical point where the bond lifetime may plateau or eventually rupture

20   under extreme force-load (Fig. 1B). Finally, atomic force microscopy performed with

21   purified rat muscle myosin II heavy meromyosin (HMM) fragments (35) and optical

22   tweezer experiments with single muscle myosin II ensembles (36, 37) have suggested

23   that some myosin motor unbinding dynamics can be described by catch-slip bonds; which

1   have been modeled within the context of motors by considering nucleotide-binding state

2   (35). Catch-slip bonds exhibit a biphasic response to applied force; initially force-load

3   increases the bond lifetime up to a critical point (the catch regime), after which the bond

4   lifetime decreases (the slip regime) (Fig. 1C). While biological motors may exhibit

5   complex force-dependent unbinding dynamics, these three simple scenarios cover the

6   possible fundamental behaviors well. Nevertheless, the impact of unbinding dynamics on

7   actomyosin network architecture, connectivity, and ultimately, contractility, remains

8   unknown both *in vivo* and *in silico*.

9   Published agent-based models of actomyosin networks have incorporated actin

10   filament treadmilling (17, 18, 22), filament buckling (15, 16), varied crosslinker/motor

11   ratios (15, 16, 22), and complex motor ensemble strategies (33, 34, 38–40). However,

12   the relevance of these models to force generation in actomyosin networks is limited by

13   how myosins were modeled. Specifically, many models employ simple dimeric processive

14   motors some of which translocate in the opposite direction to NMMII (15, 16, 23, 40). In

15   some cases motor ensembles were depicted either as multiple discrete binding entities

16   (each representing one or a few motor heads) or as a single binding entity (coarse-

17   grained; representing all the motors on one end of the filament). In the latter case, it is

18   difficult to calculate aggregate binding and unbinding rates that correctly depict the

19   behavior of multiple motors (22). The former is computationally intensive and may not

20   realistically depict the complex crosstalk among motor subunits in an ensemble. Thus,

21   there is no established solution for how to model the NMMII ensembles in an actomyosin

22   system in such a way that optimizes simplicity and computational time, while

23   recapitulating biological observations with maximal realism.

6

1   We sought to identify a suitable representation of NMMII that would recapitulate

2   realistic motoring and crosslinking functions, as desired to simulate the mechanisms of

3   non-muscle contractility. Using the agent-based modeling software, Cytosim (25)

4   (www.cytosim.org), we compared several approaches to modeling NMMII motors in the

5   context of contractile systems, consisting of actin-like filaments (referred to as "filaments"

6   for simplicity), NMMII-like motor ensembles, and non-motor crosslinkers as necessary to

7   general filament crosslinking and scaffold the network. Whereas previously we simulated

8   NMMII filaments as simplified, coarse-grained, motor clusters represented by single actin

9   binders on either side of stiff rods (22), here we compared such coarse-grained models

10   with simulations of motor ensembles where motors were discretized and independent of

11   each other. We also compared the behaviors of ensembles with motor domains exhibiting

12   slip, catch, and catch-slip bond dynamics. We demonstrated that all three of these

13   approximations can generate contractile networks, though they differ dramatically in their

14   outcome, particularly in the macroscopic contraction rates and network order. We offer

15   recommendations on motor modeling for optimization of calculation time, connectivity,

16   and biological rigor.

17

18   **MATERIALS AND METHODS**

19   *Cytosim base code*

20   Cytosim, an Open Source Brownian motion C++ simulation program (25), was

21   used to perform all agent-based simulations in this work. Within Cytosim, filaments are

22   modeled as segmented lines, with bending elasticity as determined by the persistence

1   length of F-actin, this is ~15 µm, resulting in a bending modulus of 0.06 pN·µm². Filament

2   movements are determined by an over-dampened Langevin equation:

3   (Eq. 1) $\xi \, dx/dt = f(x, t) + B(t)$

4   This equation accounts for system viscosity, drag (ξ as determined by the size of the

5   filament) (41), thermal energy in term $B(t)$, while $f(x, t)$ includes the bending elasticity of

6   the filament and the forces exerted by connectors (25). All simulations were initiated with

7   an environmental viscosity of 1 Pa.s, similar to the viscosity of *C. elegans* zygote

8   cytoplasm (42) and a thermal energy of 4.2 pN·nm. Actin dynamics were simulated as in

9   previous models (17, 18), and include depolymerization primarily at pointed ends and

10   polymerization primarily at barbed ends, with a net treadmilling rate of 0.1 µm/s and net

11   depolymerization rate of 0.002 µm/s (43). Generic crosslinkers were modeled as rigid

12   rods with actin and NMMII binding hands branching off them. Unless otherwise noted, all

13   filament binders were modeled to have force-dependent unbinding rates. Unbinding

14   dynamics of crosslinkers and scaffolds were modeled according to Kramers' theory:

15   (Eq. 2) $k_{off}(F) = k^0_{off} \exp(F_t/F_0)$

16   Here k_0 is the unloaded unbinding rate, F_0 is the characteristic unbinding force, and F_t is

17   the force felt by crosslinkers across their links at time t.

18   NMMII motor head unbinding dynamics were calculated by one of several methods

19   which yield either slip bond, catch bond, or catch-slip bond dynamics. Motoring speed

20   was calculated at each simulation frame by the formula: $V_t = V_0 (1 - F_t / F^0_{stall})$ (except for in

21   the case of parallel cluster model (PCM) motors; where V_0 is the unloaded motor speed,

22   F_0 is the stall force, and F_t is the load force, projected on the filament, at timepoint t. NMMII

8

1 complexes were simulated as bipolar couples with actin-binding motoring domains

2 attached at either end of a filament. Each actin-binding motor domain was modeled to

3 simulate the dynamics of one or several NMMII motoring heads (between 1-16) for total

4 NMMII valence of 12-32 motors (1–3).

5 The code of Cytosim was modified to enable new functionalities as follows:

6   1) Catch bond approximation using the Parallel Cluster Model (PCM):

7 (Eq. 3) $k_{off}(F) = \sum_{j=1}^{Nt} \frac{1}{r(j)} \prod_{k=1}^{j-1} \frac{g(k)}{r(k)}$

8 Where Nt is the number of motors, r(j) is the reverse rate of motor unbinding given j post-

9 power stroke motors, g(k) is the forward rate of binding given k post-power stroke motors

10 and r(k) is the reverse rate of unbinding given k post-power stroke motors; all of which

11 are described in greater detail within their original work (33).

12   2) Bound-motor mean velocity approximation for PCM:

13 (Eq. 4) $v_{eff} = \sum_{i=1}^{Nt} v_i \, \hat{p}_i(\infty)$

14 Where v_i is the complex velocity given i bound motors and $\hat{p}_i(\infty)$ the probability of an

15 average i bound motors over infinite time (33).

16   3) Catch-slip bond approximation:

17 (Eq. 5) $k_{off}(F) = k^0_{off} [\alpha_{catch} \exp(-F\, x_{catch}/k_B T) + \beta_{slip} \exp(F\, x_{slip}/k_B T)]$

18 Where k^0_{off} is the unbinding rate at rest, F is the force on motors, x_{catch} and x_{slip} are

19 characteristic myosin II bond lengths, α_{catch} and β_{slip} are constants that weigh the catch

20 and slip components, k_B is Boltzman's constant, and T is temperature (34, 35).

21   4) Simple catch bond approximation:

9

1   (Eq. 6) $k_{off}(F) = k^0_{off} [\alpha_{catch} \exp(-F \, x_{catch} / k_B T)]$

2   Which is a reduction of Eq. 5 where only the catch component is considered. General

3   parameters used in most simulations are described and referenced in Table S1 of the

4   Supporting Material.

5

6   MM1: *Single motor force-load simulations*

7   (See Supplemental SINGLE_MOTOR configuration file for details). Simulations

8   (Fig. S1E; Movie 1) were set up to mimic laser trap force-load assays of single motors. A

9   single filament with actin-like properties was immobilized in a horizontal orientation into

10   the center of a periodic space 2 μm × 200 nm and subjected to a tug-or-war between a

11   motor and a passive Hookean element. This passive element remained attached to the

12   filament at all times. The motor was given a high binding rate to allow for more binding

13   events (and therefore measurements) but its unbinding dynamic and motoring

14   parameters followed exactly the different NMMII models. As these simulations run the

15   motor pulls the filament leftward, loading the passive element and the motor alike.

16   Simulations were run for 100,000 frames with 1ms timesteps. At each step Cytosim output

17   the load experienced by the motor along with its calculated unbinding rate and velocity.

18   These data were plotted to visualize the effective force-load (Fig. 1A-D) and force velocity

19   (Fig. 1E-F).

20

21   MM2: *Translocating ensemble simulations*

1   (See Supplemental ENSEMBLE_TRANSLOCATION configuration file). To

2   measure were set up to measure the movement of motor ensembles without interference

3   from load and connectivity, we simulated motor ensembles, generated as monopolar

4   complexes, that could bind to only one filament per binder at a time (Movie 2). Motors,

5   either discrete or coarse-grained, were arrayed on one end of a stiff rod representing half

6   a NMMII ensemble. Immobile filaments 12.1 µm in length were placed horizontally, all

7   parallel with right-pointing plus (barbed) ends. Motor ensembles were initially placed on

8   the left side and allowed to translocate for 200 seconds along a periodic space 12 µm

9   long. Ensemble movement speed was evaluated from positions recorded every 100ms

10   and was calculated as follows: Positional information about all motor ensemble

11   backbones (the "myosin fiber") was pooled with information about the binding-state of all

12   binders attached to each ensemble fiber backbone. Translocation speed was calculated

13   for an ensemble only when the preceding time frame and the current time frame showed

14   at least one of its 'motors' bound to an immobilized filament. Translocation was then

15   calculated as the change in x-position (in nanometers) over time (each frame is 1 second

16   apart). Average translocation was calculated per ensemble over the duration of the

17   simulation. A population average and standard deviation were calculated for 200

18   ensembles of each type.

19   For visualization, kymographs were rendered in FIJI (ImageJ). The simulation state

20   was rendered every ten milliseconds, and the PNG images imported in FIJI. A line 12 µm

21   in length was drawn over one of the immobilized filaments in each simulation and the

22   'Multi Kymograph' plugin was used to construct a kymograph for 300 timepoints from each

23   simulation. Bound motor ensembles were visualized as grey dots, resulting in

11

1   kymographs of streaks or lines moving from left to right (position) down the y-axis (time)

2   of the generated images.

3   Motor ensemble binding percentage was calculated for all motors on all like-

4   ensembles at each time point of the simulation, as well as for all ensembles as a unit (an

5   ensemble was considered bound so long as 1 of its binders was actively bound to an

6   immobilized filament). Averages and standard deviations were then calculated for each

7   population of ensembles.

8

9   MM3: *Filament patch contractile system simulations*

10   (See Supplemental FILAMENT_PATCH configuration file). The simulations (Fig.

11   3B; S2; Movie 3) generated filament patches in a 2-dimensional circular space the size

12   of a fission yeast cell (radius of 1.5 μm) and seeded with motors and crosslinkers. Based

13   on estimates for fission yeast contractile rings (44, 45), we seeded 360 dynamic actin-like

14   filaments of length 1.0±0.3 μm, which depolymerize at a rate of 2nm/s, in random

15   orientations within the circular space. 360 motor ensembles and variable numbers of

16   crosslinkers, from 1,000 to 12,000, were then added and allowed to bind filaments before

17   the simulations were run. We used a circle-fitting method (described below) to estimate

18   the contractile rate in terms of a radial speed in nm/s. Tension was estimated in these

19   patches along virtual planar sections, rotated over 360 degrees in increments of 10

20   degrees. At each plane Cytosim reports the tension across all fibers intercepting the

21   plane. Tension reported is the average across all planes for each simulation or sets of

22   simulations. Maximal radial contractile speed was reported for all individual simulations

1   of the same ensemble type but with varying amounts of crosslinkers. The number of

2   crosslinkers allowing for maximal patch contractility was that which led to the highest

3   maximum contractile speed for all simulations of like-ensembles. Five simulations were

4   then run with the amount of crosslinker generating peak contractility for each ensemble

5   type and total network connectivity was calculated for these contractile networks (See

6   MM7).

7

8   MM4: *Periodic linear contractile system simulations*

9   (See Supplemental LINEAR_NETWORK configuration file). The simulations

10 shown in Fig. 4 used periodic boundary conditions to prohibit the network from shortening,

11 to estimate the force produced by the contractile network. The 2D simulation space was

12 periodic in the X-direction but not in Y with dimensions that roughly match the fission

13 yeast contractile ring at the onset of contractility: length equals 9.42 μm, 360 actin

14 filaments, 360 motor ensembles, and 1000-3000 crosslinkers (44, 45). The amount of

15 crosslinker was selected based on peak contractility curves generated in patch network

16 analysis (see MM3). Periodic simulations were run for 400 seconds of simulated time,

17 during which time most linear networks ruptured, marked by formation of a filament-free

18 gap and recoil of the network into clusters. Periodic network simulations were analyzed

19 for several features including time of rupture, local tension at the future rupture point,

20 global tension, and number of motors bound. These analyses were performed by

21 processing Cytosim's reports in MATLAB. Briefly, a plane parallel to the Y-axis was

22 scanned, with 100 nm steps, across the simulated space at each simulation time point.

23 At each position, the tension values for all filaments intersecting the plane were summed

1   to estimate a total tension at the current plane. Global tension was calculated as the

2   average of all scanned planes for each time point. Rupture was detected when no

3   intersecting filaments were reported for at least one plane. The position of the rupture

4   point was saved and the local tension at this position was plotted.

5

6   MM5: *Contractile ring simulations*

7   (See Supplemental CONTRACTILE_RING configuration file). The simulations

8   shown on Fig. 6 (Movie 5) of a 2D contractile ring were set up in a circular space with a

9   radius of 1.5 μm. Environmental parameters were as in our actin walking simulations. At

10 initiation, the space was populated with 360 actin filaments of 1 ± 0.3 μm long, and 5000

11 generalized crosslinkers. Actin filaments were placed within 60 nm of a circle of radius

12 1.490 μm, tangent to the circle. The crosslinkers were placed just overlapping and outside

13 of the actin filaments. The simulation was allowed to generate binding events without

14 moving the filaments for 2 seconds, and then 360 myosin ensembles were added to the

15 ring space. Following another 2 seconds during which only binding and unbinding could

16 occur, the Brownian dynamics were enabled, and run for 400 seconds. For simplicity, the

17 abundance of components was constant throughout the simulations. However, unbound

18 components could diffuse far enough away from the ring to never reincorporate, and thus

19 be non-productive. Actin filaments were dynamically treadmilling with net polymerization

20 at one end and net depolymerization at the other (0.002 μm/s). For more details see the

21 sample code.

22

1

2

3   MM6: *Circle-fitting of contractile patch simulations*

4   Patch and ring network (MM4 and MM5) closure dynamics were quantified by

5   estimating the speed of radial change. Given the variable nature of these networks in our

6   simulations, an average radius R was first calculated for all time points. From Cytosim,

7   we first exported coordinates for the centers of all myosin ensembles at each time point

8   as .CSV files. These CSV files were reorganized for readability then ported as tabular

9   data into MATLAB (TheMathWorks) as structures consisting of coordinate matrices for

10   each frame of simulated data.

11   The Pratt method (46) was then used to fit a circle to each set of coordinate points

12   representing the network, allowing us to estimate R(t), from which we derived raw radial

13   speed:

14   (Eq. 7) $[R(t + \delta) - R(t)]/\delta$

15   Where radius is recorded in μm, and δ is the timestep in second. We also used the radius

16   measurements to calculate network closure percentages as:

17   (Eq. 8) $100 [1 - R(t) / R(0)]$

18   The ring perimeter was also calculated for each frame. Simulated networks

19   constricted in noisy, sometimes off-center as well. As such, we reduced fitting-error noise

20   by performing a moving average of speed, radius and perimeter data with a window of

21   five frames. We also controlled for the possibility of a network closing partway and then

1 reopening after losing connectivity or tension. This was done by calculating the derivative

2 of the closure percentage and finding values that were smaller than -1%/min^2 suggesting

3 significant relaxation of the network. If significant relaxation was recorded at frame *n* data

4 from frames 1 to *n-1* were kept for calculation of speed while all other data were

5 discarded. Similarly, to prevent noise from data that occurred after full network

6 constriction, we discarded data from beyond 95% closure.

7 Once all data were smoothened for each individual simulation, we combined the

8 datasets for all like simulations and calculated average and standard deviation of speed,

9 percent closure and perimeter. Average speed data were smoothened via a five-frame

10 window moving average, as before (22).

11

12 MM7: *Network Connectivity Estimations*

13 We extended Cytosim report functions to export meaningful connectivity data

14 specifically for this project. First, to report motor ensemble-based connectivity (λ), we

15 coded in a function that found all motor subunits from a myosin ensemble and reported

16 the unique identifier of all associated filaments (one filament per attached motor). These

17 data, in CSV format, were then ported to MATLAB where a simple function detected the

18 number of unique filaments interacting with each motor ensemble at each time point. The

19 interaction number was then averaged for all motor ensembles throughout the simulation

20 or up until 80% closure was achieved. The average number of unique filaments attached

21 to an ensemble, Γ, was then used to calculate its contribution to connectivity:

22 (Eq. 9) $\lambda = \Gamma(\Gamma - 1)/2.$

16

The λ for all motor ensembles were summed to calculate the final connectivity provided by NMMII ensembles. The same approach described above was used to sum connectivity of non-motor crosslinkers. The different connectivity numbers were summed to calculate the total network connectivity in these simulations.

MM8: *Statistical analysis of data*

All replicate data were reported as a mean ± one standard deviation from the mean. Comparison of mean data between different bond type and ensemble discretization or coarse-graining was performed by use of unpaired t test analysis in GraphPad Prism8 (www.graphpad.com).

RESULTS

Different bond types generate different force-binding curves in silico

By default, Cytosim filament-binders follow Bell's Law and Kramers' theory (31) to calculate force-dependent unbinding of components; unbinding rate increases exponentially as force is applied to filament binders, as seen in biological slip bonds. Since myosins have been observed to exhibit catch- and catch-slip bond behavior (32, 35), we first modified Cytosim base code to include models for the force-dependent regimes of catch bonds and catch-slip bonds. Cytosim was adapted such that different force-dependent unbinding equations could be selected for any class of filament-binders. At each simulated timestep, forces were calculated and used to estimate the unbinding

1   rate of the individual components based on which method was selected. To verify our

2   implementation, we first set up simulations to mimic *in vitro* single motor laser trap

3   experiments (see Methods MM1). Briefly, single simulated motors pulled against a

4   passive Hookean link, load on the motors was varied, and unbinding rate was reported.

5   Importantly, motors unbinding according to the three different models performed markedly

6   different from one another (Figure 1A-C). The previously published Parallel Cluster Model

7   (PCM) resulted in emergent catch-bond dynamics (Figure 1D), but with an unbinding rate

8   roughly 20-fold lower than that observed with any of the other models. Thus, bond types

Figure 1. Single motor force-dependent dynamics. A-D) Different laws relating force to unbinding rates, used by Cytosim, and obtained here directly from the implementation. A) With slip bond dynamics unbinding rate exponentially increases with force. B) With catch bond dynamics, the unbinding rate decreases exponentially with force. C) Catch-slip bond dynamics show an initial catch-like behavior, here below ≈5pN, and a slip-like behavior at higher force. D) The Parallel Cluster Model (PCM) exhibits catch bond dynamics with low unbinding rates. E) The force-velocity relationship for all but PCM bond types follows Eq. 10, where load and velocity are linearly related. F) The force-velocity relationship for PCM bond type, as characterized by Eq. 4, is exponential. Each curve is built from ~100,000 individual data points extracted from running simulations.

9   other than simple slip-bonds can now be implemented in Cytosim.

1   *PCM motors have different force-velocity profiles*

2   The effect of force on velocity in Cytosim can be calculated by converting force

3   exerted on the motor into load; which is assistive if directed in the direction of motor

4   translocation, and resistive otherwise. Displacement (D) is then calculated as:

5   (Eq. 10) $D = \delta \left(v_0 + f|v_0|/F_s \right)$

6   Where v_0 is the unloaded speed, f is the directional load, and F_s is the stall force of the

7   motor. This results in linear force-velocity curves for single motors (Figure 1E, Figure S1

8   in the Supporting Material) of the catch, slip and catch-slip types.

9   However, the PCM approach includes an independent way of calculating an

10   average effective velocity, v_{eff}, that considers the average behavior of a binder with i

11   bound motors (Eq. 4). Since v_{eff} is calculated as the average behavior of a stochastic

12   ensemble, force is considered as a positive net value instead of being treated as

13   directional load on the motor ensemble. The result is a force-velocity curve with an

14   exponential drop-off, which reaches zero velocity closer to 20 pN of force per motor

15   (Figure 1F), compared with a linear relationship with the same derivative at zero (Figure

16   1E). Both methods of calculating single motor load-dependent velocity result in curves

17   with characteristic behaviors comparable to measurements made *in vitro* for muscle

18   myosin and *in vivo* for motors (47, 48). Thus, *in silico* motors can recapitulate force-

19   dependent behavior demonstrated *in vitro.*

20

21

1   *Discrete ensembles translocate on immobilized filaments*

2   We next built motor ensembles akin to structures reported from *in vitro*

3   reconstituted mammalian NMMII (1–3) and tested them in translocation assays *in silico*.

4   Ensembles of each motor type were constructed by permanently coupling motor agents

5   to one end of a long stiff rod. Ensembles were generated in a monopolar formation, unlike

6   bipolar ensembles *in vitro*, to simplify translocation simulations and reduce the potential

7   of ensembles interacting with and binding to multiple filaments at once. Fully discretized

8   monopolar versions of each ensemble were constructed by attaching 16 motor agents to

9   one end of a stiff rod (Figure 2A).

10   We first simulated discretized ensemble translocation on immobilized filaments for

11   all three bond types and the PCM model (Movie 2). Catch and catch-slip bonding

12   ensembles motored with similar, though statistically distinguishable speeds of 130±4

13   nm/s (Figure 2B, F) and 135±4 nm/s (Figure 2D, F) respectively. Both of these

14   translocation speeds fall in the reported range of ~133±75 nm/s for *in vitro* reconstituted

15   NMMIIA ensembles (1). Slip bonding motor ensembles also translocate well, though at

16   121±6 nm/s (Figure 2C, F), significantly slower than expected. Finally, PCM discretized

17   motors translocate even more slowly at 51±11 nm/s (Figure 2E, F). *In vitro* reconstituted

18   NMMIIA ensembles were previously shown to be highly processive, remaining bound

19   actin fibers through most of their translocation time (1). Thus, we set out to calculate the

20   average percent of time bound for each type of motor ensemble and found that PCM

21   ensembles were the best binders, remaining bound 99.6±0.41% of total simulation time.

22   Catch-slip bond ensembles were second best at binding, remaining bound 87±2.88% of

23   total simulation time. Catch and slip bond ensembles were markedly worse binders with

1. 76±4.85% and 59±4.74% binding percentages respectively (Figure 2G). Thus, while all

2. motor bond types were capable of binding to and translocating on filaments, only catch

3. and catch-slip bond ensembles appeared to recapitulate established behavior of
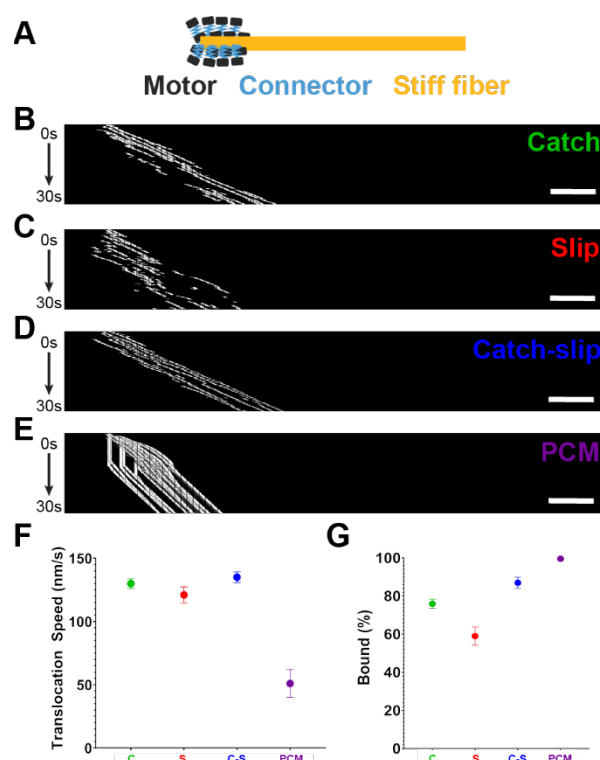
4. reconstituted NMMII ensembles.

Figure 2. Discretized motor ensemble translocation on immobilized filaments. A) Schematic representation of a monopolar motor ensemble where individual NMMII-like motors (grey) are affixed to one end of a stiff rod representing NMMII bundled tails (yellow), by springs (blue). B-E) Kymographs of catch bond (B), slip bond (C), catch-slip bond (D) and PCM (E) ensembles (grey) translocating on immobilized filaments (not shown). All kymographs extend over 12 μm (x-axis) and 30s (300 frames) in duration (y-axis). F) Translocation speeds for each ensemble type shown in B-E. G) Binding percentage (over total time) for each ensemble type shown in B-E. Points show mean; bars show standard deviation. Sample size is 5 simulations with 40 ensembles each for a total of 200 data points for each case. Scale bars are 1 μm.

5.

6. *Catch-slip bond ensembles contract patch networks fastest*

7. After establishing that motors with all bond types can translocate under low load,

8. we next characterized how different motor ensembles behave in contractile networks. For

9. these more physiologically relevant networks, we simulated bipolar ensembles with 16

discretized motors on either end of the stiff rod (1–3; Figure 3A). Bipolar motor ensembles were then seeded into simulations bearing randomly oriented actin-like filaments, which treadmill and depolymerize over time, and generic crosslinkers that can bind motor ensemble rods and actin-like filaments, similar to anillin proteins (49). Based on measurements from fission yeast cytokinetic rings (35), motor ensembles and filaments were present at a 1:1 ratio (360 of each), and 1,000-12,000 crosslinkers were included. Varying crosslinker amount affected the maximum contractile speed for all three bond types, including PCM catch bonds (Figure 3B; Figure S2 of the Supporting Material). Interestingly, only catch-slip and PCM motor ensembles exhibited a peak in contractility at intermediate crosslinker concentration (within the presented range) as predicted from cell biological, *in vitro* reconstitution, and earlier *in silico* work (15, 16, 22, 23; Figure 3C), which was around 3000 crosslinkers or ~8-fold more crosslinker than motor ensembles per fiber for catch-slip, and around 2000 crosslinkers or ~5-fold more crosslinker than motors per fiber for PCM. Catch and slip bond ensembles revealed optimal contractility with lower connectivity when crosslinker sweeps were repeated with 200-1200, both peaking around 1000 crosslinkers (Figure S3A of the Supporting Material), or ~3-fold more crosslinkers than motors per fiber. When we compared what crosslinker level allowed maximum contraction speed for all bond types, we saw that all but the PCM model exhibited the same initial behavior up to ~1000 crosslinkers. After this point, slip and catch bond ensembles appeared to lose productive force generation and dropped off in contractile speed with peaks at 87±3.97 nm/s for catch bond and 70±4.97 nm/s for slip bond ensembles. Catch-slip ensembles, in contrast, peaked at 106±2.97 nm/s. PCM

1 ensembles were the least effective force generators with peak contractile rates of 8±0.37
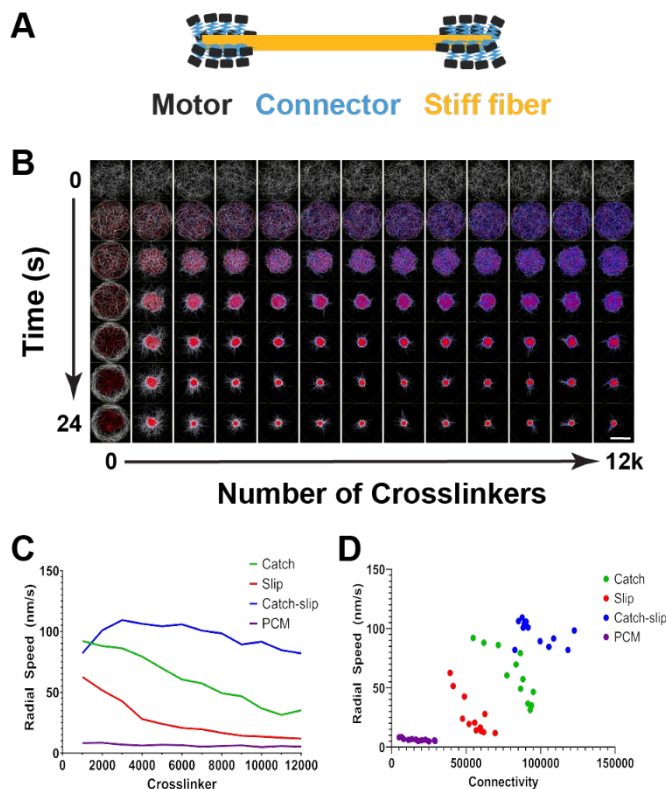
2 nm/s (Figure 3C).

3

Figure 3. Contractile patch simulations of discretized motor ensembles. Schematic representation of a bipolar motor ensemble where individual NMMII-like motors (grey) are affixed to both ends of a stiff rod representing NMMII bundled tails (yellow), by springs (blue). B) Representative simulations of contractile patches. Actin-like filaments (white) are seeded with motor ensembles (red) and varying amount of crosslinkers (blue) ranging from 0 to 12,000 (along the x-axis). Simulation snapshots are shown from top (0s) to bottom (24s) with 4s intervals. C) Radial closure speed (in nm/s) of contractile patches for each ensemble type as a function of crosslinker amount. D) Radial speeds for all conditions of each ensemble type (dots) as a function of calculated total connectivity (see Methods MM7) of the patch networks. Scale bar (bottom right) is 1.5μm.

4 We next compared the effect of total connectivity, calculated as the sum

5 connectivity contributions of motor ensembles and crosslinkers (see Methods MM7).

6 Similarly, catch-slip bonding ensembles were able to generate productive force with

7 higher connectivity than ensembles with either of the other bond types (Figure 3D).

8 Maximal contractility occurs for catch-slip bond ensembles with connectivity of

9 79,000±4,900, at 59,000±7,200 for catch bond ensembles, at 41,000±9,200 for slip bond

10 ensembles, and at 6,900+120 for PCM ensembles. Thus, PCM ensembles do not achieve

1   contractility even in highly connected networks, despite being better at binding in

2   translocation simulations. Interestingly, discretized PCM ensembles do not confer much

3   connectivity themselves, but were robust bundlers unlike other ensemble types, as

4   evidenced by significant filament alignment not seen for other ensemble simulations

5   (Figure S3B) and quantified by network directionality analysis which revealed peak order

6   of ~0.6 for PCM ensembles and ~0.37-0.47 for all others (Figure S3C-E; Movie 6). Thus,

7   even in these simplified contractile systems we saw different contractile dynamics with all

8   four different motor bond models.

9

10   *Motor ensemble dynamics on linear actin networks*

11   The stark contrast among motor bond types on contracting patches suggested that

12   these variably-binding ensembles would also achieve different levels of tension. To

13   characterize the effect of motor bond type on tension generation, we constructed periodic

14   linear networks that generate contractile tension but cannot contract. We simulated linear

15   bundles the length of the *S. pombe* contractile ring circumference, in a 2D space with

16   periodic horizontal boundaries. As with the patch simulations, we modeled 360 actin-like

17   filaments that treadmill and depolymerize over time, with 360 motor ensembles.

18   Crosslinker amounts were based on that which allowed maximum contraction speed in

19   patch simulations. In these linear network simulations, tension built up, marked by a

20   thinning of the filament band, which then ruptured in all (n = 20) simulations run with slip,

21   catch and catch-slip bond ensemble simulations, but only in 12 out of the 20 PCM

22   simulations (Figure 4A; Movie 4). As with actin patch simulations, catch-slip bond

23   ensembles generated the highest global tension, which was 3 to 30-fold higher than that

24

1   of the other discretized ensemble simulations (Figure 4B). In addition, a higher percent of

2   catch-slip bond ensembles were bound than all other ensemble types (Figure 4C).

3   Interestingly, PCM ensembles were only bound around 29%. This can be explained in

4   part by the overall lower tension generated by linear networks bearing PCM ensembles,

5   which was ~1.2 pN, 30-fold lower than that reported for catch-slip bond ensembles. PCM

6   ensembles, which behave as catch bonds, are poor binders unless significant force is

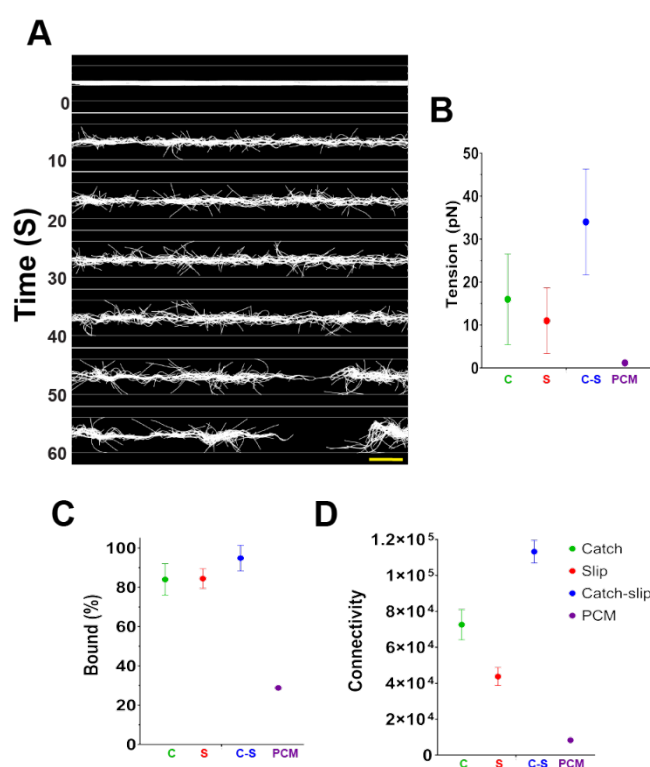7   applied to them, here these ensembles felt too little force to remain effectively bound.

Figure 4. Linear periodic contractile network simulations of discretized motor ensembles. A) Representative simulation of a linear network that is closed on itself across periodic boundaries. Actin-like filaments (white) are initially placed horizontally but in random left/right orientation and position. Motors (not shown) exerting tension eventually lead to rupture (at t=50s). Scale bar (yellow) is 1 µm. B) Average tension (before rupture) through a cross-section of the linear networks with each of the ensemble types. C) Percentages of bound motors (before rupture) for each ensemble type. D) Average total connectivity (see Method MM7) before rupture, for each of the motor types. Points show mean; bars show standard deviation. Sample size is 20 simulations for each motor ensemble type.

8   We also assessed network connectivity conferred by crosslinkers and motor

9   ensembles. Similarly to their behavior on contractile patches, catch-slip bond ensembles

10   in bundles generated the highest total connectivity, topping out at ~110,000, and PCM

11   ensembles were the lowest, topping out at ~8,000 (Figure 4D). Connectivity across all

25

1   simulations is higher than the connectivity for the same discrete ensemble type in actin

2   patches, suggesting that network architecture also contributed to total connectivity.

3

4   *Coarse-grained PCM motor ensembles generate more force than discretized PCM*

5   *ensembles*

6   Modeling motor ensembles with discretized motor domains takes full advantage of

7   the powers of agent-based modeling but is computationally costly. Indeed, NMMII

8   ensembles have conventionally been fully or partially coarse-grained in agent-based

9   models (22, 33, 39). We therefore next set out to compare fully coarse-grained ensembles

10   with the different bond types to their discretized counterparts in our simulation setups. For

11   PCM ensembles, this was done by changing a single parameter representing ensemble

12   size that dictates the number of motors being estimated as a single entity by statistical

13   mechanics (33). Increasing the coarse-graining of PCM ensembles (while keeping the

14   total number of motors depicted at 16 per side) significantly increased translocation speed

15   and processivity (Figure 5A). Filament patches with coarse-grained PCM ensembles had

16   ~3-fold lower connectivity and 13-fold higher contractile speed than patches with

17   discretized PCM ensembles (Table S3 of the Supporting Material). Similarly, linear actin

18   networks with coarse-grained PCM ensembles generated 15 times as much tension as

19   simulations with discretized PCM ensembles and always (n = 20) ruptured within 9±2.86

20   seconds of simulated time compared to only 12 out of 20 that ruptured at 382±20.15

21   seconds for discretized motors. In addition, a greater proportion of coarse-grained PCM

22   ensembles were bound (98.1±0.43%) versus 28.8±0.16% of discretized ensembles

1 (Table S4 of the Supporting Material), which is not surprising given the higher force

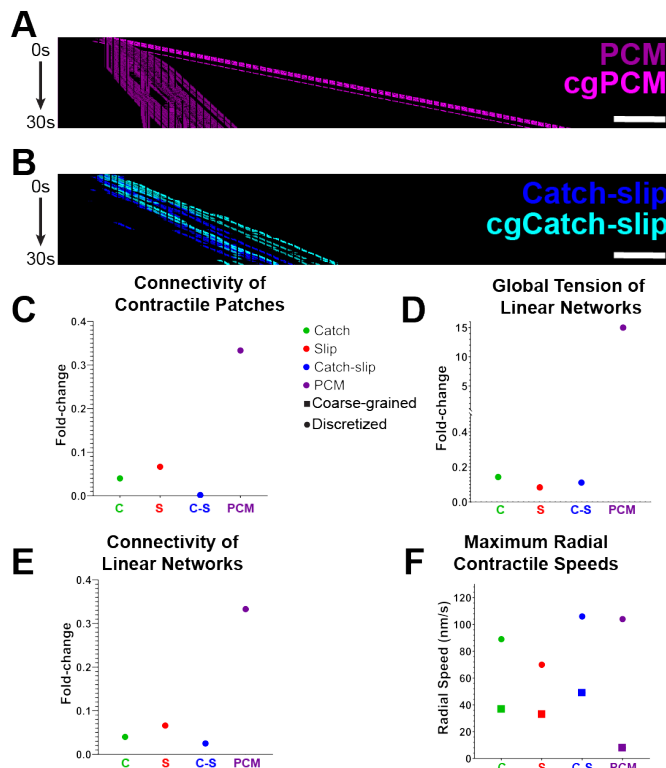2 produced by networks with coarse-grained ensembles.

Figure 5. Comparison of discretized and coarse-grained motor ensembles. A) Kymograph comparing discrete (light grey) and coarse-grained (dark grey) PCM ensembles translocating on immobilized filaments. B) Kymograph of discrete (dark blue) versus coarse-grained (light blue) catch-slip ensembles showing similar kinematics. Kymographs are 12μm (x-axis) by 30s (300 frames; y-axis). C) Fold-change in global tension for contractile patches with discrete versus coarse-grained ensembles of all types. D) Fold-change in global tension for periodic linear networks with discrete versus coarse-grained ensembles of all types. E) Fold-change in Binding % on linear networks between discrete and coarse-grained ensembles of all types. Fold-changes under 1 indicate fold decrease from discretized to coarse-grained ensembles. F) Maximal radial contractile speed versus connectivity for all ensemble types. Squares show speeds for contractile networks with discretized ensembles; circles show speeds for networks with coarse-grained ensembles. Sample size is 5 simulations for all data. Standard deviations in F are too small to visualize. Scale bars are 1 μm.

3 For the PCM method, some changes in contractile dynamics arise due to different

4 binding and motoring ability conferred by the averaging of collective motor behavior.

5 However, as expected from the representation of fewer filament-binding sites on coarse-

6 grained motor ensembles, in both patch simulations and linear actin network simulations,

7 coarse-grained PCM ensembles conferred lower total network connectivity compared to

8 discretized PCM ensembles. Therefore, connectivity could also explain some of the

9 differences in contractile dynamics.

1   *Coarse-grained ensembles of non-PCM motors achieve less contractility*

2   We expected that coarse-graining of all motor ensemble types would generally

3   reduce network connectivity due to a decrease in the number of available filament-binders

4   per ensemble. By generating coarse-grained ensembles with binding and motoring

5   behavior comparable to discrete ensembles with the same motor type, we could test

6   whether the changes in connectivity resulting from coarse-graining contributed

7   significantly to changes in ensemble and network dynamics. Thus, we next set out to

8   generate coarse-grained ensembles of catch, slip, and catch-slip bond types. These

9   methods require parameter values which have not yet been measured for aggregated

10   motors. Thus, we first used immobilized filament ensemble translocation simulations (see

11   Methods MM2) to test a range of values for several parameters to establish the coarse-

12   grained versions of ensembles for each bond type that translocated similarly to

13   discretized ensembles of the same bond type. Binding and unbinding rates, as well as

14   unloaded speed and stall force, were all swept in translocation simulations. Qualitatively,

15   coarse-grained ensembles exhibited similar dynamics to their discretized counterparts

16   (Figure 5A, B; Movie 7). Statistical analysis revealed no difference within coarse-grained

17   and discretized pairs, in terms of either translocation speed or ensemble binding

18   percentages (Table S2 of the Supporting Material).

19   Coarse-grained ensembles seeded onto filament patches conferred lower

20   connectivity than the discretized counterparts for each bond type: 15-fold decrease in

21   connectivity for slip bond ensembles, 20-fold decrease for catch bond ensembles, and

22   30-fold decrease for catch-slip bonding ensembles at peak contractile speeds (Figure

23   5C). This decrease in connectivity occurs in parallel with a ~2-2.5-fold drop in contractile

28

1 speeds for all three bond types (Figure 5F). Linear networks with coarse-grained

2 ensembles of the three types showed similar drops in connectivity (Figure 5E), and

3 tension generation (Figure 5D), which resulted in delayed rupture. Given the artificially

4 high binding rates and low force-dependent unbinding rates of coarse-grained

5 ensembles, it is not surprising that all three bond types exhibited high ensemble bound

6 percentages. Coarse-grained ensembles with catch and catch-slip bonds were virtually

7 indistinguishable at 98.9±1.5% and 98.2±1.2%, with slip ensembles not much lower at

8 94.6±1.1% (Table S4). In sum, coarse-graining of all non-PCM ensembles resulted in a

9 reduction in connectivity, as expected, along with drops in tension generation and

10 contractile speed.

11

12 **DISCUSSION**

13 *Summary*

14   In this work we compared the behavior of NMMII-like motor ensembles using four

15 modeling strategies covering three unbinding behaviors; catch, catch-slip, and slip bonds.

16 We further compared the effects of modeling ensembles of all four strategies as either

17 fully discretized entities with individual motor agents or as fully coarse-grained entities

18 leaving only two motoring agents per NMMII ensemble, behaving as a collection of

19 motors. We showed that all unbinding laws affect motor binding and translocation speeds

20 as well as network properties such as contractile speed and connectivity. Importantly,

21 coarse-graining of ensembles significantly alters network connectivity and global

29

1   contractile rates independently of an effect on individual motor speed and binding

2   dynamics for all four models.

3

4   *PCM ensembles*

5   As previously reported (33), catch-bond behavior is an emergent property of

6   motors operating according to the parallel cluster model. Here we expand this observation

7   to the emergence of catch dynamics for ensembles of 32 motors, whether motors are fully

8   coarse-grained or fully discretized. However, coarse-graining does alter the binding time

9   both at the individual agent level and at the ensemble level. PCM ensembles can generate

10 more force as coarse-graining increases due to an increase in the number of bound

11 motors and therefore an increase in the average effective velocity. Due to a higher

12 tension, the catch-bond behavior of coarse-grained PCM ensembles ensures that they

13 are better binders in both patch and periodic filament network simulations. Compared to

14 all other motor strategies, discretized PCM ensembles are the least effective force-

15 generators but coarse-grained PCM ensembles are among the best at force generation

16 (only catch-slip ensembles are better).

17 Two caveats exist here, however. First, PCM motors were simulated using

18 parameters estimated from muscle myosins which are known to have different biophysical

19 properties than non-muscle myosins. Future work should therefore carefully adapt the

20 PCM method with NMMII parameters. This is important, especially given that all other

21 motor types were simulated using parameters estimated for NMMIIA (34). Second,

22 network connectivity, which has been repeatedly shown to be important for contractile

1   dynamics (15, 16, 22, 23), is lower for both modes of PCM ensemble simulation. In the

2   case of the more processive coarse-grained PCM ensembles, the network connectivity is

3   decreased because each ensemble can bind a maximum of two actin-like filaments

4   instead of ~20-30. While this may be compensated *in silico* by adding more non-motor

5   crosslinkers, we lack the ability to discern the direct effect of motor-based connectivity on

6   contractile dynamics. We therefore suggest that the coarse PCM method is ideal for fast

7   and robust simulation of large processive motor ensembles so long as questions about

8   connectivity need not be addressed.

9

10   *Slip bonding motor ensembles*

11   Slip bond motor ensembles are much poorer force generators than PCM, catch or

12   catch-slip bonding ensembles with the same level of coarse-graining. This result is not

13   surprising given the inherent decrease in binding lifetime as a contractile network comes

14   under tension. Fully discrete slip ensembles are fast motors when they are bound, largely

15   due to their quick unbinding that likely often happens before the motor reaches stall force,

16   but the same characteristic makes these motors such poor binders that they exhibit little

17   processivity in our immobilized filament simulations. At very low ratios of non-motor

18   crosslinkers to motor ensembles, slip bond ensembles can produce contractile speeds

19   around 50-60 nm/s with peak tension around 100 pN across actin patches. Coarse-

20   graining slip bond ensembles results in a significant drop in all metrics (excluding

21   unloaded binding and translocation speed, which were matched to their discretized

22   equivalent). In the case of slip bond ensembles, coarse-graining does not appear to

23   provide any benefit beyond simplifying the structure of motor ensembles and reducing

1   computation time. Use of slip bond motors in simulations would therefore be best suited

2   to modeling single motors that follows such a law.

3

4   *Catch bonding motor ensembles*

5   Catch bond motor ensembles are predicted to be good crosslinkers given their

6   inherent increase in binding lifetime as force is applied. In practice, however, we see

7   comparable binding percentage for discrete catch bond ensembles as for slip bond

8   ensembles (84±8% vs 84.4±5%) in linear actomyosin network simulations. This finding

9   could be reconciled if the force experienced by individual motors in each ensemble is low

10   for slip motors, where they will have maximal bond lifetimes, and low-intermediate for

11   catch bonds, where they may have minimal bond lifetimes. One important distinction,

12   however, is that discrete catch bond ensembles are better crosslinkers than discrete slip

13   bond ensembles, as evidenced by the 1.6-fold increase in total network connectivity in

14   catch bond ensemble simulations compared to those with slip bonds. Not surprisingly,

15   given that both coarse-grained catch and slip bonding ensembles are good binders and

16   can bind maximally two actin-like fibers, this distinction does not hold true for their coarse-

17   grained forms, which have more similar connectivity. In sum, discretized catch bond motor

18   ensembles are useful for their ability to increase network connectivity but are not the most

19   effective force generators. Increasing evidence that NMMIIB is a good crosslinker and a

20   poor force generator (1, 34) suggests that for modeling these motors, a catch bond

21   method would be suitable and perhaps more realistic than a slip bond method.

22

32

1   *Catch-slip bonding ensembles*

2   Due to the hybrid nature of their force-dependent unbinding dynamics, catch-slip

3   bond motors could be predicted to be the most versatile model. Indeed, in both patch and

4   periodic network simulations, discrete catch-slip ensembles had the highest contractile

5   speeds while also bearing the highest total connectivity. In terms of force generation,

6   contractile patches with catch-slip ensembles bore the highest tension (~8-fold higher

7   than catch or slip ensembles), but in the less permissive periodic linear network

8   simulations, tensions were more comparable (~1-1.25-fold higher only). Here again, it

9   stands to reason that since force experienced by individual motors may not be very high,

10   catch-slip motors would be better individual binders of actin-like filaments. Indeed,

11   comparison of individual motor binding shows that catch-slip bond motors are bound

12   54±5.2% of the time versus 30±5.6% for catch and 16±2.7% for slip bond motors. As with

13   slip and catch bonding ensembles, coarse-graining of catch-slip bond ensembles renders

14   them less effective force generators and drastically reduces total network connectivity

15   (2,800±80 pN compared to 113,00±6300 pN for discrete). As such, there is no inherent

16   benefit to coarse-graining catch-slip bonding ensembles. Within a biological context,

17   discrete catch-slip bond ensembles could be the most robust way of simulating non-

18   processive motors that form processive collectives in ensembles. This robustness was

19   shown previously in simulations of gliding filaments on clusters of fixed motors (34), and

20   here we show the same behavior in the context of generic actomyosin contractile

21   systems. Therefore, we suggest that discretized catch-slip bond ensembles provide the

22   best *in silico* approximation for NMMIIA ensembles in the context of contractile systems

23   where connectivity is considered.

1   *Coarse-graining ensembles*

2   Generally, coarse-graining NMMII ensembles reduces complexity and can speed

3   up computation of simulations by 2 to 3-fold. However, our work shows that coarse-

4   grained ensembles do not generate as much connectivity as discretized ensembles of the

5   same bond type. Comparison among the coarse-grained forms of all bond types revealed

6   insignificant differences between their total connectivity, which averaged around 2,900

7   connections. This stark contrast to huge differences in connectivity between the

8   discretized versions of each bond type revealed that coarse-graining not only greatly

9   diminishes network connectivity, but also reduces the effect of bond type on connectivity.

10   This is not surprising given the total reduction in motoring fiber binders by 16-fold (from

11   32 per ensemble to 2 per ensemble). It is important to note that coarse-grained versions

12   of each bond type ensemble still generate vastly different contractile dynamics from one

13   another. This is evident by both contractile rates and tension estimates for filament

14   patches and for rupture timing and tension estimates for linear contractile networks.

15   Overall, with the exception of PCM ensembles, which have different emergent properties

16   based on the method of calculating effective bound velocity and binding dynamics,

17   coarse-graining conserves the general relationships between the motor bond types.

18   Catch-slip bond ensembles remain the most effective force-generators (ignoring PCM)

19   and slip ensembles the worst binders. Coarse-graining ensembles can therefore be

20   considered a useful strategy for simulations that seek to describe general principles of

21   contractility in large contractile systems.

22

23

On contractile rings

One long-term application of the work presented herein is to build a predictive model of actomyosin contractility in the cytokinetic contractile ring, where NMMII is the major force generator and also contributes to connectivity (10, 20, 50). Recent *in silico* work on contractile ring dynamics has focused on modeling fission yeast cytokinesis (11, 38–40, 51). Modeling this contractile system is especially powerful due to the availability of published measurements of the absolute amounts of cytoskeletal components present on the fission yeast cytokinetic ring (44, 45). Much of this modeling work has used simplified coarse-grained or partially coarse-grained motors to represent NMMII ensembles (39, 40). As such, connectivity of the actomyosin network has largely been
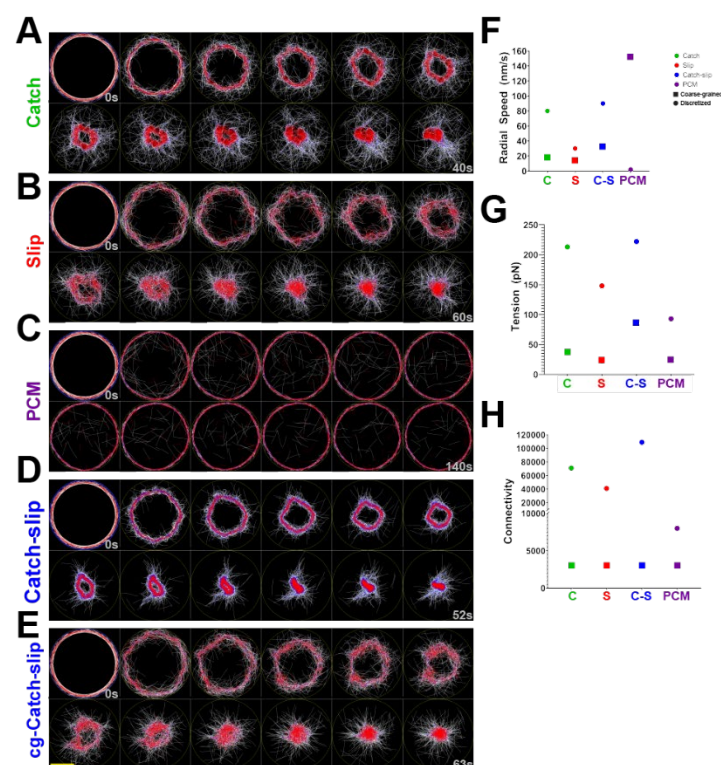

Figure 6. Contractile ring simulations. A-E) Representative timeframes from simulations of fission yeast-sized contractile rings with all four ensemble types (A-D) and coarse-grained catch-slip motor ensembles (E). Scale bar (yellow; bottom left) is 1μm. F) Maximum radial contractile speed shown for single simulations of rings shown in A-E of each ensemble type with discretized and coarse-grained motors. G) Maximum tension calculated from rings bearing ensembles of each bond type in both discretized and coarse-grained formats. H) Total connectivity of contractile rings bearing ensembles of each bond type with discretizes or coarse-grained motors. Dots in all plots represent data from contractile rings with discretized ensembles; squares represent data from rings with coarse-grained ensembles.

1   simplified. We sought preliminary evidence that the discretized catch and catch-slip motor

2   ensembles we described above will yield contractile ring simulations with more realistic

3   network connectivity, even though the model of the ring is generalized and simplistic,

4   lacking for instance an anchorage to a moving plasma membrane-like boundary.

5   Modeling contractile rings bearing each of our different types of motor ensembles

6   revealed similar relationships to those presented above for patches and linear networks

7   (Movie 8; Movie 5). Discretized catch-slip bond ensembles provided the most realistic

8   combination of force generation, contractile speed, and connectivity (Fig. 6F-H).

9   Discretized catch bond ensembles are not far behind in terms of speed and tension, with

10   slip bond and PCM ensembles performing the least optimally. These findings suggest

11   that the motor behaviors presented here will be relevant to a broad diversity of actomyosin

12   networks where connectivity is important for force transmission.

13

14   *Perspectives*

15   By focusing on the motors, this study can lead to more accurate simulations of

16   biological contractile networks. However, several further steps can be taken to increase

17   biological accuracy beyond the scope of motor ensemble simulations presented here.

18   Actin dynamics are complex and can vary for many reasons. In the work presented here

19   we incorporated actin polymerization and depolymerization at both ends of the filament

20   along with a net treadmilling rate. Actin filament buckling can cause increased severing

21   (13) depolymerization (52). In the current work we do not include either of these dynamic

22   processes. Severing is a function already included in Cytosim, bending-dependent

23   depolymerization is not. Future work to characterize the effects of these more complex

1   actin-dynamics in contractile systems will undoubtedly provide valuable insight into the

2   mechanisms of contractility. One important component of contractile ring dynamics that

3   remains mostly ignored is the contribution of the plasma membrane to the mechanics of

4   contraction. Recent models have begun incorporating fluid membranes (40), but motor

5   ensembles in this study were significantly coarse-grained. Our work in describing the

6   effects of coarse-graining on network connectivity suggests that future work with

7   deformable membranes would further benefit from using discretized motor ensembles.

8

AUTHOR CONTRIBUTIONS

D.B.C., A.S.M, and F.N designed the research. D.B.C. carried out most of the simulations and data analysis. M.G. performed some simulations and assisted with data analysis. D.B.C. and A.S.M. wrote the manuscript with support from F.N.

13

14

ACKNOWLEDGEMENTS

21

SUPPORTING CITATIONS

References (53–58) appear in the Supporting Material.

24

25

REFERENCES

1. Melli, L., N. Billington, S.A. Sun, J.E. Bird, A. Nagy, T.B. Friedman, Y. Takagi, and J.R. Sellers. 2018. Bipolar filaments of human nonmuscle myosin 2-A and 2-B have distinct motile and mechanical properties. Elife. 7: 1–25.

2. Nagy, A., Y. Takagi, N. Billington, S.A. Sun, D.K.T. Hong, E. Homsher, A. Wang, and J.R. Sellers. 2013. Kinetic characterization of nonmuscle myosin IIB at the single molecule level. J. Biol. Chem. 288: 709–722.

3. Billington, N., A. Wang, J. Mao, R.S. Adelstein, and J.R. Sellers. 2013. Characterization of three full-length human nonmuscle myosin II paralogs. J. Biol. Chem. 288: 33398–33410.

4. Agarwal, P., and R. Zaidel-Bar. 2019. Diverse roles of non-muscle myosin II contractility in 3D cell migration. Essays Biochem. 63: 497–508.

5. Heuzé, M.L., G.H.N. Sankara Narayana, J. D'Alessandro, V. Cellerin, T. Dang, D.S. Williams, J.C. Van Hest, P. Marcq, R.-M. Mège, and B. Ladoux. 2019. Myosin II isoforms play distinct roles in adherens junction biogenesis. Elife. 8.

6. Maciver, S.K. 1996. Myosin II function in non-muscle cells. Bioessays. 18: 179–82.

7. Even-Ram, S., A.D. Doyle, M.A. Conti, K. Matsumoto, R.S. Adelstein, and K.M. Yamada. 2007. Myosin IIA regulates cell motility and actomyosin-microtubule crosstalk. Nat. Cell Biol. 9: 299–309.

8. Wang, F., M. Kovacs, A. Hu, J. Limouze, E. V. Harvey, and J.R. Sellers. 2003. Kinetic Mechanism of Non-muscle Myosin IIB. J. Biol. Chem. 278: 27439–27448.

9. Kovács, M., F. Wang, A. Hu, Y. Zhang, and J.R. Sellers. 2003. Functional divergence of human cytoplasmic myosin II. Kinetic characterization of the non-muscle IIA isoform. J. Biol. Chem. 278: 38132–38140.

10. Laplante, C., J. Berro, E. Karatekin, A. Hernandez-Leyva, R. Lee, and T.D. Pollard. 2015. Three Myosins Contribute Uniquely to the Assembly and Constriction of the Fission Yeast Cytokinetic Contractile Ring. Curr. Biol. 25: 1955–1965.

11. Stachowiak, M.R., C. Laplante, H.F. Chin, B. Guirao, E. Karatekin, T.D. Pollard, and B. O'Shaughnessy. 2014. Mechanism of Cytokinetic Contractile Ring Constriction in Fission Yeast. Dev. Cell. 29: 547–561.

12. Vicente-manzanares, M., X. Ma, R.S. Adelstein, and A.R. Horwitz. 2009. Non-muscle myosin II takes centre stage in cell adhesion and migration. Nat Rev Mol Cell Biol. 10: 778–790.

13. Murrell, M.P., and M.L. Gardel. 2012. F-actin buckling coordinates contractility and severing in a biomimetic actomyosin cortex. Proc. Natl. Acad. Sci. U. S. A. 109: 20820–5.

14. Lenz, M., T. Thoresen, M.L. Gardel, and A.R. Dinner. 2012. Contractile Units in Disordered Actomyosin Bundles Arise from F-Actin Buckling. Phys. Rev. Lett. 108: 238107.

15. Ennomani, H., G. Letort, C. Guerin, J.L. Martiel, W. Cao, F. Nedelec, E.M. De La Cruz, M. Thery, and L. Blanchoin. 2016. Architecture and Connectivity Govern Actin Network Contractility. Curr. Biol. 26: 616–626.

16. Belmonte, J.M., M. Leptin, and F. Nédélec. 2017. A theory that predicts behaviors of disordered cytoskeletal networks. Mol. Syst. Biol. 13: 941.

17. Mendes Pinto, I., B. Rubinstein, A. Kucharavy, J.R. Unruh, and R. Li. 2012. Actin Depolymerization Drives Actomyosin Ring Contraction during Budding Yeast Cytokinesis. Dev. Cell. 22: 1247–1260.

18. Oelz, D.B., B.Y. Rubinstein, and A. Mogilner. 2015. A Combination of Actin Treadmilling and Cross-Linking Drives Contraction of Random Actomyosin Arrays. Biophys. J. 109: 1818–1829.

19. Ma, X., M. Kovács, M. Anne, A. Wang, Y. Zhang, and J.R. Sellers. 2012. Nonmuscle myosin II exerts tension but does not translocate actin in vertebrate cytokinesis. Proc. Natl. Acad. Sci. 109: 4509–4514.

20. Osorio, D.S., F.Y. Chan, J. Saramago, J. Leite, A.M. Silva, A.F. Sobral, R. Gassmann, and A.X. Carvalho. 2019. Crosslinking activity of non-muscle myosin II is not sufficient for embryonic cytokinesis in C. elegans. Development. : dev.179150.

21. Vasquez, C.G., S.M. Heissler, N. Billington, J.R. Sellers, and A.C. Martin. 2016. Drosophila non-muscle myosin II motor activity determines the rate of tissue folding. Elife. 5: 1–20.

22. Descovich, C.P., D.B. Cortes, S. Ryan, J. Nash, L. ZHang, P.S. Maddox, F. Nedelec, and A.S. Maddox. 2018. Cross-linkers both drive and brake cytoskeletal remodeling and furrowing in cytokinesis. Mol. Biol. Cell. 29: 622–631.

23. Ding, W.Y., H.T. Ong, Y. Hara, J. Wongsantichon, Y. Toyama, R.C. Robinson, F. Nédélec, and R. Zaidel-Bar. 2017. Plastin increases cortical connectivity to facilitate robust polarization and timely cytokinesis. J. Cell Biol. 216: 1371–1386.

24. Li, Y., J.R. Christensen, K.E. Homa, G.M. Hocky, A. Fok, J.A. Sees, G.A. Voth, and D.R. Kovar. 2016. The F-actin bundler α-actinin Ain1 is tailored for ring assembly and constriction during cytokinesis in fission yeast. Mol. Biol. Cell. 27: 1821–1833.

25. Nedelec, F., and D. Foethke. 2007. Collective Langevin dynamics of flexible cytoskeletal fibers. New J. Phys. 9.

26. Freedman, S.L., S. Banerjee, G.M. Hocky, and A.R. Dinner. 2017. A Versatile Framework for Simulating the Dynamic Mechanical Structure of Cytoskeletal Networks. Biophys. J. 113: 448–460.

27. Chandrasekaran, A., A. Upadhyaya, and G.A. Papoian. 2019. Remarkable structural transformations of actin bundles are driven by their initial polarity, motor activity, crosslinking, and filament treadmilling. PLoS Comput. Biol. 15: e1007156.

28. Hafner, A.E., J. Krausser, and A. Šarić. 2019. Minimal coarse-grained models for molecular self-organisation in biology. Curr. Opin. Struct. Biol. 58: 43–52.

29. Nicholas, M.P., F. Berger, L. Rao, S. Brenner, C. Cho, and A. Gennerich. 2015. Cytoplasmic dynein regulates its attachment to microtubules via nucleotide state-switched mechanosensing at multiple AAA domains. Proc. Natl. Acad. Sci. 112: 6371–6376.

30. Guo, S.-K., X.-X. Shi, P.-Y. Wang, and P. Xie. 2019. Force dependence of unbinding rate of kinesin motor during its processive movement on microtubule. Biophys. Chem. 253: 106216.

31. Walcott, S. 2008. The load dependence of rate constants. J. Chem. Phys. 128: 215101.

32. Coluccio, L.M., and M.A. Geeves. 1999. Transient kinetic analysis of the 130-kDa myosin I (MYR-1 gene product) from rat liver. A myosin I designed for maintenance of tension. J. Biol. Chem. 274: 21575–21580.

33. Erdmann, T., P.J. Albert, and U.S. Schwarz. 2013. Stochastic dynamics of small ensembles of non-processive molecular motors: the parallel cluster model. J. Chem. Phys. 139: 175104:1-175104–27.

34. Stam, S., J. Alberts, M.L. Gardel, and E. Munro. 2015. Isoforms Confer Characteristic Force Generation and Mechanosensation by Myosin II Filaments. Biophys. J. 108: 1997–2006.

35. Guo, B., and W.H. Guilford. 2006. Mechanics of actomyosin bonds in different nucleotide states are tuned to muscle contraction. Proc. Natl. Acad. Sci. U. S. A. 103: 9844–9.

36. Nishizaka, T., H. Miyata, H. Yoshikawa, S. Ishiwata, and K. Kinosita. 1995. Unbinding force of a single motor molecule of muscle measured using optical tweezers. Nature. 377: 251–254.

37. Yamada, A., A. Mamane, J. Lee-Tin-Wah, A. Di Cicco, C. Prévost, D. Lévy, J.F. Joanny, E. Coudrier, and P. Bassereau. 2014. Catch-bond behaviour facilitates membrane tubulation by non-processive myosin 1b. Nat. Commun. 5: 3624.

38. Bidone, T.C., H. Tang, and D. Vavylonis. 2014. Dynamic network morphology and tension buildup in a 3D model of cytokinetic ring assembly. Biophys. J. 107: 2618–2628.

39. Bidone, T.C., W. Jung, D. Maruri, C. Borau, R.D. Kamm, and T. Kim. 2017. Morphological Transformation and Force Generation of Active Cytoskeletal Networks. PLoS Comput. Biol. 13.

40. Nguyen, L.T., M.T. Swulius, S. Aich, M. Mishra, and G.J. Jensen. 2018. Coarse-

grained simulations of actomyosin rings point to a nodeless model involving both unipolar and bipolar myosins. Mol. Biol. Cell. 29: 1318–1331.

41.   Tirado, M.M., and J.G. de la Torre. 1979. Translational friction coefficients of rigid, symmetric top macromolecules. Application to circular cylinders. J. Chem. Phys. 71: 2581–2587.

42.   Daniels, B.R., B.C. Masi, and D. Wirtz. 2006. Probing Single-Cell Micromechanics In Vivo : The Microrheology of C . elegans Developing Embryos. 90: 4712–4719.

43.   Pollard, T.D. 1986. Rate Constants for the Reactions of ATP- and ADP-Actin with the Ends of Actin Filaments. J. Cell Biol. 103: 2747–2754.

44.   Wu, J.-Q., and T.D. Pollard. 2005. Counting cytokinesis proteins globally and locally in fission yeast. Science. 310: 310–4.

45.   Courtemanche, N., T.D. Pollard, Q. Chen, N. Haven, and N. Haven. 2017. Avoiding artifacts when counting polymerized actin in live cells with Lifeact-fluorescent fusion proteins. 18: 676–683.

46.   Pratt, V. 1987. Direct least-squares fitting of algebraic surfaces. ACM SIGGRAPH Comput. Graph. 21: 145–152.

47.   Shtridelman, Y., T. Cahyuti, B. Townsend, D. DeWitt, and J.C. Macosko. 2008. Force-velocity curves of motor proteins cooperating in vivo. Cell Biochem. Biophys. 52: 19–29.

48.   Hill, A.. 1938. The heat of shortening and the dynamic constants of muscle. Proc. R. Soc. London. Ser. B - Biol. Sci. 126: 136–195.

49.   Piekny, A.J., and A.S. Maddox. 2010. The myriad roles of Anillin during cytokinesis. Semin. Cell Dev. Biol. 21: 881–891.

50.   Yang, F., Q. Wei, R.S. Adelstein, and P.J. Wang. 2012. Non-muscle myosin IIB is essential for cytokinesis during male meiotic cell divisions. Dev. Biol. 369: 356–61.

51.   Vavylonis, D., J.-Q. Wu, S. Hao, B. O'Shaughnessy, and T.D. Pollard. 2008. Assembly mechanism of the contractile ring for cytokinesis by fission yeast. Science. 319: 97–100.

52.   Yogurtcu, O.N., J.S. Kim, and S.X. Sun. 2012. A mechanochemical model of actin filaments. Biophys. J. 103: 719–27.

53.   Isambert, H., P. Venier, A. Maggs, A. Fattoum, R. Kassab, D. Pantaloni, and M. Carlier. 1995. Flexibility of actin filaments derived from thermal fluctuations. Effect of bound nucleotide, phalloidin, and muscle regulatory proteins. J. Biol. Chem. 270: 11437–11444.

54.   Umemoto, S., and J.R. Sellers. 1990. Characterization of in vitro motility assays using smooth muscle and cytoplasmic myosins. J. Biol. Chem. 265: 14864–14869.

55. Thoresen, T., M. Lenz, and M.L. Gardel. 2013. Thick filament length and isoform composition determine self-organized contractile units in actomyosin bundles. Biophys. J. 104: 655–665.

56. Niederman, R., and T.D. Pollard. 1975. Human Platelet Myosin. J. Cell Biol. 67: 72–92.

57. Sinard, J.H., W.F. Stafford, and T.D. Pollard. 1989. The mechanism of assembly of Acanthamoeba myosin-II minifilaments: minifilaments assemble by three successive dimerization steps. J. Cell Biol. 109: 1537–1547.

58. Shutova, M.S., W.A. Spessott, C.G. Giraudo, and T. Svitkina. 2014. Endogenous species of mammalian nonmuscle myosin IIA and IIB include activated monomers and heteropolymers. Curr. Biol. 24: 1958–1968.

FIGURE LEGENDS

Figure 1. Single motor force-dependent dynamics. A-D) Different laws relating force to unbinding rates, used by Cytosim, and obtained here directly from the implementation. A) With slip bond dynamics unbinding rate exponentially increases with force. B) With catch bond dynamics, the unbinding rate decreases exponentially with force. C) Catch-slip bond dynamics show an initial catch-like behavior, here below ≈5pN, and a slip-like behavior at higher force. D) The Parallel Cluster Model (PCM) exhibits catch bond dynamics with low unbinding rates. E) The force-velocity relationship for all but PCM bond types follows Eq. 10, where load and velocity are linearly related. F) The force-velocity relationship for PCM bond type, as characterized by Eq. 4, is exponential. Each curve is built from ~100,000 individual data points extracted from running simulations.

Figure 2. Discretized motor ensemble translocation on immobilized filaments. A) Schematic representation of a monopolar motor ensemble where individual NMMII-like motors (grey) are affixed to one end of a stiff rod representing NMMII bundled tails (yellow), by springs (blue). B-E) Kymographs of catch bond (B), slip bond (C), catch-slip bond (D) and PCM (E) ensembles (grey) translocating on immobilized filaments (not shown). All kymographs extend over 12 µm (x-axis) and 30s (300 frames) in duration (y-axis). F) Translocation speeds for each ensemble type shown in B-E. G) Binding percentage (over total time) for each ensemble type shown in B-E. Points show mean; bars show standard deviation. Sample size is 5 simulations with 40 ensembles each for a total of 200 data points for each case. Scale bars are 1 µm.

Figure 3. Contractile patch simulations of discretized motor ensembles. Schematic representation of a bipolar motor ensemble where individual NMMII-like motors (grey) are affixed to both ends of a stiff rod representing NMMII bundled tails (yellow), by springs (blue). B) Representative simulations of contractile patches. Actin-like filaments (white) are seeded with motor ensembles (red) and varying amount of crosslinkers (blue) ranging from 0 to 12,000 (along the x-axis). Simulation snapshots are shown from top (0s) to bottom (24s) with 4s intervals. C) Radial closure speed (in nm/s) of contractile patches for each ensemble type as a function of crosslinker amount. D) Radial speeds for all conditions of each ensemble type (dots) as a function of calculated total connectivity (see Methods MM7) of the patch networks. Scale bar (bottom right) is 1.5µm.

Figure 4. Linear periodic contractile network simulations of discretized motor ensembles. A) Representative simulation of a linear network that is closed on itself across periodic boundaries. Actin-like filaments (white) are initially placed horizontally but in random left/right orientation and position. Motors (not shown) exerting tension eventually lead to rupture (at t=50s). Scale bar (yellow) is 1 µm. B) Average tension (before rupture) through a cross-section of the linear networks with each of the ensemble types. C) Percentages of bound motors (before rupture) for each ensemble type. D) Average total connectivity (see Method MM7) before rupture, for each of the motor types. Points show mean; bars show standard deviation. Sample size is 20 simulations for each motor ensemble type.

Figure 5. Comparison of discretized and coarse-grained motor ensembles. A) Kymograph comparing discrete (light grey) and coarse-grained (dark grey) PCM ensembles translocating on immobilized filaments. B) Kymograph of discrete (dark blue) versus coarse-grained (light blue) catch-slip ensembles showing similar kinematics. Kymographs are 12µm (x-axis) by 30s (300 frames; y-axis). C) Fold-change in global tension for contractile patches with discrete versus coarse-grained ensembles of all types. D) Fold-change in global tension for periodic linear networks with discrete versus coarse-grained ensembles of all types. E) Fold-change in Binding % on linear networks between discrete and coarse-grained ensembles of all types. Fold-changes under 1 indicate fold decrease from discretized to coarse-grained ensembles. F) Maximal radial contractile speed versus connectivity for all ensemble types. Squares show speeds for contractile networks with discretized ensembles; circles show speeds for networks with coarse-grained ensembles. Sample size is 5 simulations for all data. Standard deviations in F are too small to visualize. Scale bars are 1 µm.

Figure 6. Contractile ring simulations. A-E) Representative timeframes from simulations of fission yeast-sized contractile rings with all four ensemble types (A-D) and coarse-grained catch-slip motor ensembles (E). Scale bar (yellow; bottom left) is 1µm. F) Maximum radial contractile speed shown for single simulations of rings shown in A-E of each ensemble type with discretized and coarse-grained motors. G) Maximum tension calculated from rings bearing ensembles of each bond type in both discretized and coarse-grained formats. H) Total connectivity of contractile rings bearing ensembles of each bond type with discretizes or coarse-grained motors. Dots in all plots represent data from contractile rings with discretized ensembles; squares represent data from rings with coarse-grained ensembles.

Movie 1. Simulations of force-dependent single motor dynamics. Simulations for all four motor types are shown in the proximity of a single actin-like filament (white) which is permanently bound to a single Hookean spring (orange). Solid color indicates binding of catch bond (green), slip bond (red), catch-slip bond (blue), or PCM (purple) discrete single motors; brighter coloring indicates bound state. Timesteps are 1 millisecond apart; total simulation time is 0.8 seconds shown at 40 frames/second.

Movie 2. Ensemble translocation on immobilized filaments. Simulation shows monopolar ensembles bearing the four discrete motor types (16 motors per ensemble; catch (green), slip (red), catch-slip (blue), or PCM (purple)). Purple PCM dots only intermittently appear due to poor binding. Immobilized filaments are dashed grey lines. Yellow lines indicate the rod to which motors are affixed. Motors bind (solid dots) and translocate from left to right. Timesteps are 100 milliseconds apart; total simulation time is 80 seconds shown at 40 frames/second.

Movie 3. Contractile patches with different crosslinker amounts. Three simulations of contractile patches (white filaments) within 2D circular spaces (yellow circles). Total number of motor ensembles (red) is the same across all three but crosslinker amount (blue) increases from left to right. Crosslinker amount affects network structure and

contractile dynamics. Timesteps are 0.5 seconds apart; total simulation time is 30 seconds shown at 12 frames/second.

Movie 4. Linear periodic contractile networks. Simulations of linear networks made of white filaments and blue crosslinkers bearing catch-slip (top) or PCM (bottom) motor ensembles in red. Timesteps are 0.5 seconds apart; total simulation time is 50 seconds shown at 12 frames/second.

Movie 5. Contractile ring dynamics with discretized catch-slip bond motor ensembles. Simulation shows a contractile ring formed by seeding filaments (white) in a circular pattern tangential to the simulation space (yellow circle) with crosslinkers (blue) and motors (red). Timesteps are 0.5 seconds apart; total simulation time is 54 seconds shown at 12 frames/second.

Movie 6. Highly structured and bundled filaments in patch simulations. Simulation of a contractile patch (as in Movie 3) bearing discrete PCM motor ensembles. These patches are not very contractile and instead form large bundles of mostly linear filaments over time. Only filaments (white) are shown to highlight the bundling of filaments and to show input data for directionality analysis. Timesteps are 0.5 seconds apart; total simulation time is 203 seconds shown at 12 frames/second.

Movie 7. Ensemble translocation of discrete versus coarse-grained ensembles. Simulation of discrete (dark blue) or coarse-grained (sky blue) catch-slip ensembles translocating on immobilized actin-like filaments. Dots appear when motors are bound and actively translocating from left to right. Yellow lines represent ensemble rods to which motors are bound. Free parameters for coarse-grained ensembles were fit via parameter sweeps to behave indistinguishably from discretized versions. Timesteps are 100 milliseconds apart; total simulation time is 80 seconds shown at 40 frames/second.

Movie 8. Contractile ring dynamics with discretized catch bond motor ensembles. Simulation shows a contractile ring formed by seeding filaments (white) in a circular pattern tangential to the simulation space (yellow circle) with crosslinkers (blue) and motors (red). Timesteps are 0.5 seconds apart; total simulation time is 43 seconds shown at 12 frames/second.

Table S1. General Simulation Parameters

Parameter: Value	Comments	Reference
Simulation		
Viscosity: 1 N.s/m^2	*C. elegans* embryo cytoplasm	(1)
Temperature: 0.0042 pN.um		
Time-step: 0.5-1 ms		
Actin-like Filaments		
Quantity: 360	Estimate from *S. pombe* measurements	(2, 3)
Length: 1.0 ± 0.3 μm		(2)
Rigidity: 0.06 pN.μm^2		(4)
Barbed end growth speed: 0.1 μm/s		(5)
Pointed end growth speed: 0.002 μm/s		(5)
Barbed end shrinking speed: 0.004 μm/s		(5)
Pointed end shrinking speed: 0.1 μm/s		(5)
Motor Subunits (Non-PCM) (Parameters listed for discrete motors of all but PCM method.		
Binding rate: 0.2 /s		(6)
Binding range: 60 nm	within an order of magnitude of apparent motor head reach	(7)
Unbinding rate: 1.71/s	k_0	(6)
Unbinding force: 5 pN	F_d	(8)
Unbinding relationship	Variable; based on bond-type	(6, 9–11); Eq. 5-6
Max speed: 150 nm/s	V_0	(12, 13)
Stall force: 3.85 pN	F^0_{stall}	(8, 14)
Force-speed relationship	$$D = v_0 \partial t + l|v_0|\partial t / F_s$$	Eq. 10
Stiffness: 1-200 pN/μm	Empirical	(15)
Parallel Cluster Model (PCM)		
Binding rate: 0.2 /s	Listed as k_01 for PCM calculations	(6)
Binding range: 60 nm		(7)
Unbinding rate: 1.71 /s	Listed as k_20 for PCM calculations	(6)
Unbinding relationship		(11); Eq. 3
Max Speed: 600 nm/s	V_0	
Stall force: 12.3	Estimated from Erdmann simulations	(11)
Force-speed relationship	$V_{eff} = \sum_{i=1}^{Nt} v_i \hat{p}_i(\infty)$; must be less than or equal to V_0	(11); Eq. 4
Motor Ensembles		
Quantity: 360	Estimate scaled up from *S. pombe* measurements	(2, 3)
Valence: 32	Simulated as 2 actin-binding agents of (n/2) motors in Aggregate method)	(12)
Length: 300 nm		(7, 12, 16–18)
Rigidity: 100 pN.μm^2	Single fiber represents all myosin tails	
Duty ratio: NA		
Diffusion: set by Langevin	Ensembles are simulated as fiber backbones with motors attached at each end. As such their diffusion is calculated by the over-dampened Langevin equation	
Anillin-like Crosslinker		
Quantity: [100-12000]	Performed parameter sweeps to establish optimal amount	
Length: 40 nm		
Binding rate: 10/s		
Binding range: 50 nm	Empirical	(15)

Unbinding rate:	0.3 /s for myosin; 0.1 / s for actin	
Unbinding force: 5 pN	Empirical	
Stiffness: 100 pN/µm	Empirical	

Table S2. Ensemble Translocation Simulations

Ensembles	Translocation Speed	% Bound (ensembles)
Catch	130±3.84	76±4.85
cg-Catch	130±2.85	76±2.4
Slip	121±6.39	87±2.88
cg-Slip	121±5.04	87±1.46
Catch-slip	135±4.17	59±4.74
cg-Catch-slip	135±2.48	59±3.87
PCM	51±11	100±0.41
cg-PCM	299±0.61	98±0.7

Table S3. Contractile Patch Simulations

Ensemble	Max Speed	Tension	Connectivity
Catch	89±3.97	-150±35.32	59,000±7,200
cg-Catch	37±2.09	-64±4.56	2,700±70
Slip	70±4.97	-110±46.54	41,000±9,200
cg-Slip	33±2.93	-54±5.85	2,700±80
Catch-slip	106±2.97	-900±82.08	79,000±4,900
cg-Catch-slip	49±2.87	-100±7.51	2,800±60
PCM	8±0.37	-10±2.23	6,900±130
cg-PCM	104±6.69	-210±6.52	2,800±50

Table S4. Linear Periodic Network Simulations

Ensemble	Max Tension	% Bound (binders)	% Bound (ensembles)	Connectivity
Catch	11±13	29.6±5.6	84.0±8.0	73,000±8,400
cg-Catch	4±5	88.6±4.3	98.2±1.2	2,900±60
Slip	7±7	15.5±2.7	84.4±5.0	44,000±5,000
cg-Slip	2±3	77.4±3.6	94.6±1.1	2,900±60
Catch-slip	42±36	54.1±5.2	94.8±6.5	113,000±6,400
cg-Catch-slip	2±3	95.9±2.2	98.9±1.5	2,900±80
PCM	5±5	1.0±0.1	28.8±0.2	8,000±700
cg-PCM	39±24	92.3±0.3	98.1±0.4	2,800±30

Table S1. General Simulation Parameters. Common parameters for elements simulated on contractile patches, linear networks and rings.

Table S2. Ensemble Translocation Simulations. Translocation speed (nm/s) and binding percentage data for all ensemble types on immobilized actin-like filaments. Numbers reported are mean ± standard deviation. Sample size is 200 ensembles for each.

Table S3. Contractile Patch Simulations. Maximum radial contractile speed (nm/s), network tension (pN) and connectivity for all ensemble types on contractile patches. Numbers reported are mean ± standard deviation. Sample size is 5 independent simulations for each.

Table S4. Linear Periodic Network Simulations. Maximum tension (pN), binding percentages, and connectivity reported for all ensemble types on linear periodic contractile networks. Numbers reported are mean ± standard deviation. Sample size is 20 simulations for each.
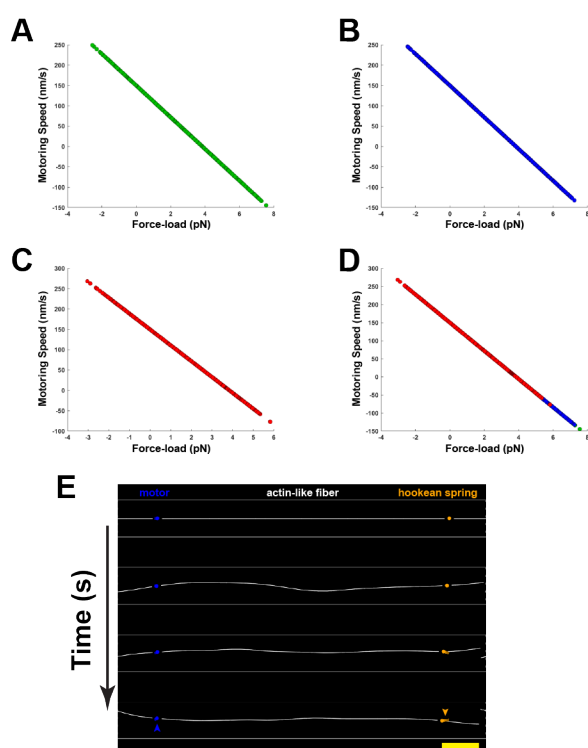

Figure S1. Single motor force-dependent velocity. A-C) The force-velocity relationship for all three (not PCM) bond types follows Eq. 10, where load and velocity are linearly related. D) Overlaid data from A-C showing they all follow the same relationship in Cytosim. Each curve is built from ~100,000 individual data points extracted from running simulations. E) Simulation timeframes from a laser trap simulation showing a motor (blue) and a Hookean spring (orange) both bound to an actin-like filament (white). As the simulation progresses the motor pulls on the fiber which causes force to be exerted on the motor by the Hookean spring holding on to the filament. Displacement of motor and spring is visualized by the 'stretching' of both components (arrowheads). Scale bar represents 100nm.

Figure S2. Contractile patch simulation comparison between discrete and coarse-grained ensembles. A- B) Representative simulations of contractile patches. Actin-like filaments (white) are seeded with discrete (A) or coarse-grained (B) motor ensembles (red) and varying amount of crosslinkers (blue) ranging from 0 to 12,000 (along the x-axis). Simulation snapshots are shown from top (0s) to bottom (24s) with 4s intervals for A and from top (0s) to bottom (88s) with 11 second intervals for B. Scale bar (bottom right) is 1.5µm.

Figure S3. Contractile patch simulation analysis. A) Finer crosslinker sweep as performed for all ensemble types, showing maximum contractile radial speed here from 200 to 1200 crosslinkers (in intervals of 200). Peaks for both catch (green) and slip (red) discretized ensemble types appear at 1000 crosslinkers. B) Directonality (order) analysis of actin-like filaments (shown in C-F) for each discrete motor ensemble type. Each dot represents the average of 5 separate simulations all ran at peak connectivity for each ensemble type taken every 0.5 seconds (401 frames; total 200.5 seconds). All but PCM (purple) simulations finished contracting before 50s (100 frames). C-F) Representative starting, middle and late timeframes from patch simulations for each discretized ensemble type. White lines are actin-like filaments; white faint circle is the simulation space. Large groups of bundled filaments are obvious in middle timepoints only for PCM simulations (arrowheads). Scale bar (bottom right) is 1μm.

Figure S1. Single motor force-dependent velocity. A-C) The force-velocity relationship for all three (not PCM) bond types follows Eq. 10, where load and velocity are linearly related. D) Overlaid data from A-C showing they all follow the same relationship in Cytosim. Each curve is built from ~100,000 individual data points extracted from running simulations. E) Simulation timeframes from a laser trap simulation showing a motor (blue) and a Hookean spring (orange) both bound to an actin-like filament (white). As the simulation progresses the motor pulls on the fiber which causes force to be exerted on the motor by the Hookean spring holding on to the filament. Displacement of motor and spring is visualized by the 'stretching' of both components (arrowheads). Scale bar represents 100nm.
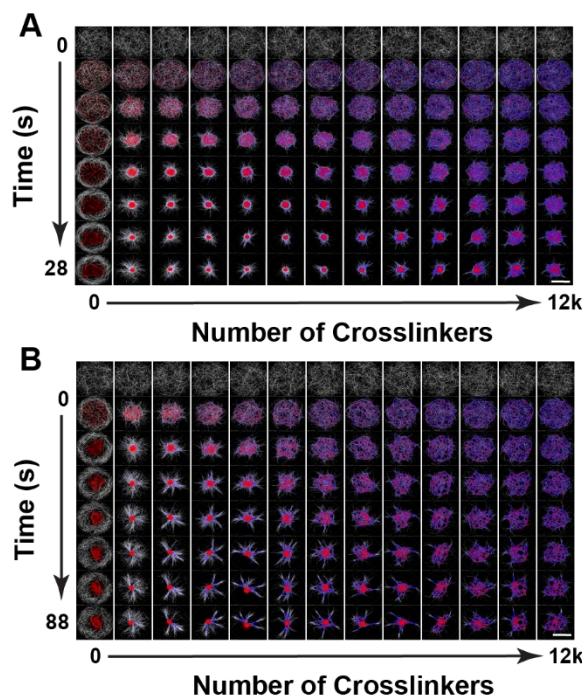
Figure S2. Contractile patch simulation comparison between discrete and coarse-grained ensembles. A- B) Representative simulations of contractile patches. Actin-like filaments (white) are seeded with discrete (A) or coarse-grained (B) motor ensembles (red) and varying amount of crosslinkers (blue) ranging from 0 to 12,000 (along the x-axis). Simulation snapshots are shown from top (0s) to bottom (24s) with 4s intervals for A and from top (0s) to bottom (88s) with 11 second intervals for B. Scale bar (bottom right) is 1.5μm.
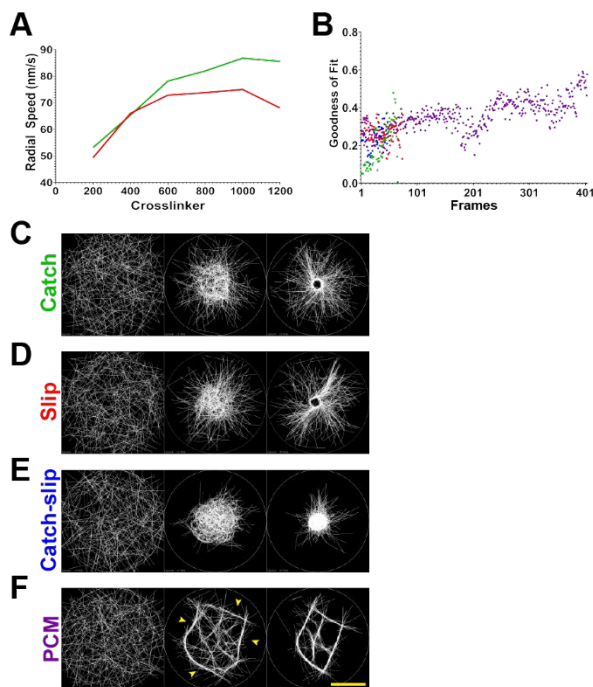
Figure S3. Contractile patch simulation analysis. A) Finer crosslinker sweep as performed for all ensemble types, showing maximum contractile radial speed here from 200 to 1200 crosslinkers (in intervals of 200). Peaks for both catch (green) and slip (red) discretized ensemble types appear at 1000 crosslinkers. B) Directonality (order) analysis of actin-like filaments (shown in C-F) for each discrete motor ensemble type. Each dot represents the average of 5 separate simulations all ran at peak connectivity for each ensemble type taken every 0.5 seconds (401 frames; total 200.5 seconds). All but PCM (purple) simulations finished contracting before 50s (100 frames). C-F) Representative starting, middle and late timeframes from patch simulations for each discretized ensemble type. White lines are

actin-like filaments; white faint circle is the simulation space. Large groups of bundled filaments are obvious in middle timepoints only for PCM simulations (arrowheads). Scale bar (bottom right) is 1µm.

SUPPORTING REFERENCES

1. Daniels, B.R., B.C. Masi, and D. Wirtz. 2006. Probing Single-Cell Micromechanics In Vivo : The Microrheology of C . elegans Developing Embryos. 90: 4712–4719.
2. Wu, J.-Q., and T.D. Pollard. 2005. Counting cytokinesis proteins globally and locally in fission yeast. Science. 310: 310–4.
3. Courtemanche, N., T.D. Pollard, Q. Chen, N. Haven, and N. Haven. 2017. Avoiding artifacts when counting polymerized actin in live cells with Lifeact-fluorescent fusion proteins. 18: 676–683.
4. Isambert, H., P. Venier, A. Maggs, A. Fattoum, R. Kassab, D. Pantaloni, and M. Carlier. 1995. Flexibility of actin filaments derived from thermal fluctuations. Effect of bound nucleotide, phalloidin, and muscle regulatory proteins. J. Biol. Chem. 270: 11437–11444.
5. Pollard, T.D. 1986. Rate Constants for the Reactions of ATP- and ADP-Actin with the Ends of Actin Filaments. J. Cell Biol. 103: 2747–2754.
6. Stam, S., J. Alberts, M.L. Gardel, and E. Munro. 2015. Isoforms Confer Characteristic Force Generation and Mechanosensation by Myosin II Filaments. Biophys. J. 108: 1997–2006.
7. Billington, N., A. Wang, J. Mao, R.S. Adelstein, and J.R. Sellers. 2013. Characterization of three full-length human nonmuscle myosin II paralogs. J. Biol. Chem. 288: 33398–33410.
8. Oelz, D.B., B.Y. Rubinstein, and A. Mogilner. Contraction of random actomyosin arrays is enabled by the combined effect of actin treadmilling and crosslinking Supporting Material. : 1–12.
9. Walcott, S. 2008. The load dependence of rate constants. J. Chem. Phys. 128: 215101.
10. Guo, S., and K.J. Kemphues. 1996. A non-muscle myosin required for embryonic polarity in Caenorhabditis elegans. Nature. 382: 455–8.
11. Erdmann, T., P.J. Albert, and U.S. Schwarz. 2013. Stochastic dynamics of small ensembles of non-processive molecular motors: the parallel cluster model. J. Chem. Phys. 139: 175104:1-175104–27.
12. Melli, L., N. Billington, S.A. Sun, J.E. Bird, A. Nagy, T.B. Friedman, Y. Takagi, and J.R. Sellers. 2018. Bipolar filaments of human nonmuscle myosin 2-A and 2-B have distinct motile and mechanical properties. Elife. 7: 1–25.
13. Umemoto, S., and J.R. Sellers. 1990. Characterization of in vitro motility assays using smooth muscle and cytoplasmic myosins. J. Biol. Chem. 265: 14864–14869.
14. Thoresen, T., M. Lenz, and M.L. Gardel. 2011. Reconstitution of Contractile Actomyosin Bundles. Biophys. J. 100: 2698–2705.
15. Ennomani, H., G. Letort, C. Guerin, J.L. Martiel, W. Cao, F. Nedelec, E.M. De La Cruz, M. Thery, and L. Blanchoin. 2016. Architecture and Connectivity Govern Actin Network Contractility. Curr. Biol. 26: 616–626.
16. Niederman, R., and T.D. Pollard. 1975. Human Platelet Myosin. J. Cell Biol. 67: 72–92.
17. Sinard, J.H., W.F. Stafford, and T.D. Pollard. 1989. The mechanism of assembly of Acanthamoeba myosin-II minifilaments: minifilaments assemble by three successive dimerization steps. J. Cell Biol. 109: 1537–1547.
18. Shutova, M.S., W.A. Spessott, C.G. Giraudo, and T. Svitkina. 2014. Endogenous species of mammalian nonmuscle myosin IIA and IIB include activated monomers and heteropolymers. Curr. Biol. 24: 1958–1968.

```
set simul SINGLE_MOTOR
{
    time_step      = 0.001
    viscosity      = 1
    tolerance      = 0.01
    kT             = 0.0042
}


%%%%%%%%%%%%%%%%%%%%%%%%%%%%%%%SPACE%%%%%%%%%%%%%%%%%%%%%%%%%%%%%%%%%%%%%


set space cell
{
    geometry       = ( strip 1 0.1)
}

new space cell

%%%%%%%%%%%%%%%%%%%%%%%%%%%%%%%%FIBERS%%%%%%%%%%%%%%%%%%%%%%%%%%%%%%%%%%%%%



set fiber actin
{
    rigidity              = 0.06
    segmentation          = 0.05
    confine               = inside, 200

    display               = ( color = white; interval = 1.0; line_width = 1; )
}

%%%%%%%%%%%%%%%%%%%%%%%%%%%%%%%%%HANDS%%%%%%%%%%%%%%%%%%%%%%%%%%%%%%%%%%%%%



set hand NMM2
{
    hold_growing_end    = 0
    hold_shrinking_end  = 0
    activity            = move

    detach_mode         = %motor parameters are specific to bond type and coarse-grain; see motor supplement

    display             = ( color = white; size = 2 )
}

set hand concrete
{
    binding_rate        = 10
    binding_range       = 0.01
    unbinding_rate      = 0
    unbinding_force     = inf
    display             = ( color = black; size = 1; )
}
```

```
%%%%%%%%%%%%%%%%%%%%%%%%%%%%%%%SINGLES%%%%%%%%%%%%%%%%%%%%%%%%%%%%%%%%%%


set single motor
{
    stiffness       = 200
    hand            = NMM2
    activity        = fixed
}

set single Concrete
{
    hand            = concrete
    stiffness       = 100
    activity        = fixed
}


%%%%%%%%%%%%%%%%%%%%%%%%%%%%%%%RUN%%%%%%%%%%%%%%%%%%%%%%%%%%%%%%%%%%%%%%


new 1 fiber actin
{
    length          = 2
    position        = 0 0
    orientation     = horizontal
}

new 1 single Concrete
{
    position        = 0.8
}

new 1 single motor
{
    position        = -0.8
}

run simul *
{
    nb_steps        = 1000
    nb_frames       = 1
    solve           = 0
}

run simul *
{
    nb_steps        = 100000
    nb_frames       = 100000


}
```

```
set simul ENSEMBLE_TRANSLOCATION
{
    time_step      = 0.001
    viscosity      = 1
    tolerance      = 0.01
    kT             = 0.0042
}
```

%%%%%%%%%%%%%%%%%%%%%%%%%%%%%%%SPACE%%%%%%%%%%%%%%%%%%%%%%%%%%%%%%%%%%

```
set space cell
{
    geometry       = ( strip 6 2 )
}

new space cell
```

%%%%%%%%%%%%%%%%%%%%%%%%%%%%%%%FIBERS%%%%%%%%%%%%%%%%%%%%%%%%%%%%%%%%%%

```
set fiber actin
{
    rigidity            = 20
    segmentation        = 1
    confine             = inside, 200
    binding_key         = 2

    display             = ( color = white; interval = 1.0; line_width = 0.5; )
}

set fiber ensemble
{
    rigidity            = 100
    segmentation        = 0.15
    binding_key         = 4
    confine             = inside, 200

    display             = ( color = yellow; interval = 1.0; line_width = 1; )
}
```

%%%%%%%%%%%%%%%%%%%%%%%%%%%%%%%HANDS%%%%%%%%%%%%%%%%%%%%%%%%%%%%%%%%%%

```
set hand NMM2
{
    hold_growing_end    = 0
    hold_shrinking_end  = 0
    activity            = move
    binding_key         = 2

    detach_mode         =%motor parameters are specific to bond type and coarse-grain; see motor supplement
```

```
    display                 = ( color = white; size = 2 )
}

set hand motor_base
{
    binding_rate        = 0
    binding_range       = 0.05
    unbinding_rate      = 0
    unbinding_force     = inf
    binding_key         = 4
    display             = ( color = gray; size = 1; )
}

set hand concrete
{
    binding_rate        = 10
    binding_range       = 0.05
    unbinding_rate      = 0
    unbinding_force     = inf
    binding_key         = 2
    display             = ( color = black; size = 1; )
}



%%%%%%%%%%%%%%%%%%%%%%%%%%%%%%SINGLES%%%%%%%%%%%%%%%%%%%%%%%%%%%%%%%%%%



set single Concrete
{
    hand        = concrete
    stiffness   = 500
    activity    = fixed
}

%%%%%%%%%%%%%%%%%%%%%%%%%%%%%%%%COUPLES%%%%%%%%%%%%%%%%%%%%%%%%%%%%%%%%%%%



set couple motor
{
    stiffness       = 200
    hand1           = motor_base
    hand2           = NMM2
    diffusion       = 0
    length          = 0.05
}

%%%%%%%%%%%%%%%%%%%%%%%%%%%%%%%%%RUN%%%%%%%%%%%%%%%%%%%%%%%%%%%%%%%%%%%%%%%%



new 16 fiber actin
{
    length          = 12.01
```

```
    position        = 0 -1.9 to 1.9
    orientation     = horizontal
    attach          = 45 Concrete, 6, plus_end, regular
    attach1         = 45 Concrete, 6, plus_end, regular
}


new 40 fiber ensemble
{
    position        = -5 0 to -5 1.8
    length          = 0.1
    orientation     = vertical
    attach          = [x] Concrete, 6, plus_end, regular % x = 1 or 16; depends on if motor is coarse-grained or discrete
}


run  200 simul *
{
    solve           = 0
}


run 200000 simul *
{
    nb_frames       = 2000

}
```

```
set simul FILAMENT_PATCH
{
    time_step      = 0.001
    viscosity      = 1
    tolerance      = 0.01
    kT             = 0.0042
}


%%%%%%%%%%%%%%%%%%%%%%%%%%%%%%%%%SPACE%%%%%%%%%%%%%%%%%%%%%%%%%%%%%%%%%%%%%%


set space cell
{
    geometry       = ( circle 1.5 )
}

new space cell

%%%%%%%%%%%%%%%%%%%%%%%%%%%%%%%%%FIBERS%%%%%%%%%%%%%%%%%%%%%%%%%%%%%%%%%%%%%%


set fiber actin
{
    rigidity              = 20
    segmentation          = 1
    confine               = inside, 200
    binding_key           = 2
    activity              = treadmill
    growing_speed         = 0.1, 0.002
    shrinking_speed       = -0.004, -0.1
    growing_force         = inf, inf


    display               = ( color = white; interval = 1.0; line_width = 1; )
}

set fiber ensemble
{
    rigidity              = 100
    segmentation          = 0.15
    binding_key           = 4
    confine               = inside, 200

    display               = ( color = red; interval = 1.0; line_width = 1; )
}

set fiber crosslinker
{
    rigidity              = 100
    segmentation          = 0.04
    binding_key           = 32
    confine               = inside, 200
```

```
    display        = ( color = blue; interval = 1.0; line_width = 1; )
}


%%%%%%%%%%%%%%%%%%%%%%%%%%%%%%%HANDS%%%%%%%%%%%%%%%%%%%%%%%%%%%%%%%%%%%


set hand NMM2
{
    hold_growing_end    = 0
    hold_shrinking_end  = 0
    activity            = move
    binding_key         = 2

    detach_mode         =%motor parameters are specific to bond type and coarse-grain; see motor supplement

    display             = ( color = white; size = 2 )
}

set hand motor_base
{
    binding_rate        = 0
    binding_range       = 0.05
    unbinding_rate      = 0
    unbinding_force     = inf
    binding_key         = 4
    display             = ( color = red; size = 1; )
}

set hand crosslinker_base
{
    binding_rate        = 0
    binding_range       = 0.05
    unbinding_rate      = 0
    unbinding_force     = inf
    binding_key         = 32
    display             = ( color = blue; size = 1; )
}

set hand crosslinker_actin
{
    binding_rate        = 10
    binding_range       = 0.05
    unbinding_rate      = 0.1
    unbinding_force     = 8
    binding_key         = 2
    display             = ( color = white; size = 1; )
}

set hand crosslinker_ensemble
{
    binding_rate        = 5
    binding_range       = 0.05
    unbinding_rate      = 0.3
```

```
    unbinding_force      = 5
    binding_key          = 4
    display              = ( color = red; size = 1; )
}
```

%%%%%%%%%%%%%%%%%%%%%%%%%%%%%COUPLES%%%%%%%%%%%%%%%%%%%%%%%%%%%%%%%%%%

```
set couple motor
{
    stiffness       = 100
    hand1           = motor_base
    hand2           = NMM2
    diffusion       = 0
    length          = 0.05
}

set couple crosslink_actin
{
    stiffness       = 20
    hand1           = crosslinker_base
    hand2           = crosslinker_actin
    diffusion       = 0
    length          = 0.01
}

set couple  crosslink_ensemble
{
    stiffness       = 20
    hand1           = crosslinker_base
    hand2           = crosslinker_ensemble
    diffusion       = 0
    length          = 0.01
}
```

%%%%%%%%%%%%%%%%%%%%%%%%%%%%%%%RUN%%%%%%%%%%%%%%%%%%%%%%%%%%%%%%%%%%%%%

```
new 360 fiber actin
{
    length          = 1.0, 0.3
    end_state       = 4, 1
}

new [x] fiber crosslinker % x is swept for all motor types from 1,000 to 12,000 unless otherwise noted
{
    length          = 0.04
    attach          = 2 crosslink_actin, 0.02, minus_end, regular
    attach1         = 1 crosslink_ensemble, 0.01, minus_end, regular
}

run  200 simul *
{
```

```
    solve           = 0
}


new 360 fiber ensemble
{
    length          = 0.3
    attach          = [x] motor, 0.02, minus_end, regular % x = 1 or 16; depends on if motor is coarse-grained or discrete
    attach1         = [x] motor, 0.02, plus_end, regular % x = 1 or 16; depends on if motor is coarse-grained or discrete
}


run  200 simul *
{
    solve           = 0
}


run 200000 simul *
{
    nb_frames       = 400


}
```

```
set simul LINEAR_NETWORK
{
    time_step      = 0.001
    viscosity      = 1
    tolerance      = 0.01
    kT             = 0.0042
}


%%%%%%%%%%%%%%%%%%%%%%%%%%%%%%%%%SPACE%%%%%%%%%%%%%%%%%%%%%%%%%%%%%%%%%%%%%%%%


set space cell
{
    geometry       = ( strip 4.712 0.5 )
}

new space cell

%%%%%%%%%%%%%%%%%%%%%%%%%%%%%%%%%FIBERS%%%%%%%%%%%%%%%%%%%%%%%%%%%%%%%%%%%%%%%%


set fiber actin
{
    rigidity              = 0.06
    segmentation          = 0.05
    confine               = inside, 200
    binding_key           = 2
    activity              = treadmill
    growing_speed         = 0.1, 0.002
    shrinking_speed       = -0.004, -0.1
    growing_force         = inf, inf
    min_length            = 0.06


    display               = ( color = white; interval = 1.0; line_width = 1; )
}

set fiber ensemble
{
    rigidity              = 100
    segmentation          = 0.15
    binding_key           = 4
    confine               = inside, 200

    display               = ( color = red; interval = 1.0; line_width = 1; )
}

set fiber crosslinker
{
    rigidity              = 100
    segmentation          = 0.04
    binding_key           = 32
    confine               = inside, 200
```

```
    display        = ( color = blue; interval = 1.0; line_width = 1; )
}


%%%%%%%%%%%%%%%%%%%%%%%%%%%%%%%%%%HANDS%%%%%%%%%%%%%%%%%%%%%%%%%%%%%%%%%%%%%%%


set hand NMM2
{
    hold_growing_end    = 0
    hold_shrinking_end  = 0
    activity            = move
    binding_key         = 2

    detach_mode         =%motor parameters are specific to bond type and coarse-grain; see motor supplement

    display             = ( color = white; size = 2 )
}

set hand motor_base
{
    binding_rate        = 0
    binding_range       = 0.05
    unbinding_rate      = 0
    unbinding_force     = inf
    binding_key         = 4
    display             = ( color = red; size = 1; )
}

set hand crosslinker_base
{
    binding_rate        = 0
    binding_range       = 0.05
    unbinding_rate      = 0
    unbinding_force     = inf
    binding_key         = 32
    display             = ( color = blue; size = 1; )
}

set hand crosslinker_actin
{
    binding_rate        = 10
    binding_range       = 0.05
    unbinding_rate      = 0.1
    unbinding_force     = 8
    binding_key         = 2
    display             = ( color = white; size = 1; )
}

set hand crosslinker_ensemble
{
    binding_rate        = 5
    binding_range       = 0.05
```

```
    unbinding_rate        = 0.3
    unbinding_force       = 5
    binding_key           = 4
    display               = ( color = red; size = 1; )
}
```

%%%%%%%%%%%%%%%%%%%%%%%%%%%%%%%%COUPLES%%%%%%%%%%%%%%%%%%%%%%%%%%%%%%%%%%

```
set couple motor
{
    stiffness      = 100
    hand1          = motor_base
    hand2          = NMM2
    diffusion      = 0
    length         = 0.05
}

set couple crosslink_actin
{
    stiffness      = 20
    hand1          = crosslinker_base
    hand2          = crosslinker_actin
    diffusion      = 0
    length         = 0.01
}

set couple  crosslink_ensemble
{
    stiffness      = 20
    hand1          = crosslinker_base
    hand2          = crosslinker_ensemble
    diffusion      = 0
    length         = 0.01
}
```

%%%%%%%%%%%%%%%%%%%%%%%%%%%%%%%%%RUN%%%%%%%%%%%%%%%%%%%%%%%%%%%%%%%%%%%%%%%

```
new 360 fiber actin
{
    length         = 1.0, 0.3
    end_state      = 4, 1
    position       = rectangle 4.7 0.06 at 0 0
    orientation    = horizontal
}

new [x] fiber crosslinker % x is between 1,000 and 3,000 depending on motor type
{
    length         = 0.04
    attach         = 2 crosslink_actin, 0.02, minus_end, regular
    attach1        = 1 crosslink_ensemble, 0.01, minus_end, regular
}
```

```
run  200 simul *
{
    solve          = 0
}

new 360 fiber ensemble
{
    length         = 0.3
    attach         = [x] motor, 0.02, minus_end, regular % x = 1 or 16; depends on if motor is coarse-grained or discrete
    attach1        = [x] motor, 0.02, plus_end, regular % x = 1 or 16; depends on if motor is coarse-grained or discrete
    position       = rectangle 4.7 0.06 at 0 0
    orientation    = horizontal
}

run  200 simul *
{
    solve          = 0
}

run 400000 simul *
{
    nb_frames     = 800

}
```

Parameters of motors are shown for each bond-type and for discrete vs coarse-grained versions of all motor ensembles.

```
set hand CATCH_DISCRETE
{
    hold_growing_end        = 0
    hold_shrinking_end      = 0
    activity                = move
    binding_key             = 2

    detach_mode             = Catch
    binding_range           = 0.06
    binding_rate            = 0.2
    unbinding_rate          = 1.71
    alpha_catch             = 0.92
    x_catch                 = 0.1

    unloaded_speed          = 0.15
    stall_force             = 3.85

    display         = ( color = white; size = 2 )
}


set hand CATCH_CG
{
    hold_growing_end        = 0
    hold_shrinking_end      = 0
    activity                = move
    binding_key             = 2

    detach_mode             = Catch
    binding_range           = 0.12
    binding_rate            = 2.48
    unbinding_rate          = 0.9
    alpha_catch             = 0.92
    x_catch                 = 0.1

    unloaded_speed          = 0.145
    stall_force             = 4

    display         = ( color = white; size = 2 )
}


set hand SLIP_DISCRETE
{
    hold_growing_end        = 0
    hold_shrinking_end      = 0
    activity                = move
    binding_key             = 2
```

```
    detach_mode          = Slip
    binding_range        = 0.06
    binding_rate         = 0.2
    unbinding_rate       = 1.71
    unbinding_force      = 5

    unloaded_speed       = 0.15
    stall_force          = 3.85

    display              = ( color = white; size = 2 )
}


set hand SLIP_CG
{
    hold_growing_end     = 0
    hold_shrinking_end   = 0
    activity             = move
    binding_key          = 2

    detach_mode          = Slip
    binding_range        = 0.12
    binding_rate         = 1.32
    unbinding_rate       = 0.8
    unbinding_force      = 15

    unloaded_speed       = 0.137
    stall_force          = 5

    display              = ( color = white; size = 2 )

}


set hand CATCHSLIP_DISCRETE
{
    hold_growing_end     = 0
    hold_shrinking_end   = 0
    activity             = move
    binding_key          = 2

    detach_mode          = CatchSlip
    binding_range        = 0.06
    binding_rate         = 0.2
    unbinding_rate       = 1.71
    alpha_catch          = 0.92
    x_catch              = 0.607681
    alpha_slip           = 0.08
    x_slip               = 0.097229

    unloaded_speed       = 0.15
    stall_force          = 3.85
```

```
    display                 = ( color = white; size = 2 )
}


set hand CATCHSLIP_CG
{
    hold_growing_end        = 0
    hold_shrinking_end      = 0
    activity                = move
    binding_key             = 2

    detach_mode             = CatchSlip
    binding_range           = 0.12
    binding_rate            = 3.6
    unbinding_rate          = 0.8
    alpha_catch             = 0.92
    x_catch                 = 0.607681
    alpha_slip              = 0.08
    x_slip                  = 0.097229

    unloaded_speed          = 0.146
    stall_force             = 5

    display                 = ( color = white; size = 2 )

}


set hand PCM_DISCRETE
{
    hold_growing_end        = 0
    hold_shrinking_end      = 0
    activity                = move
    binding_key             = 2

    detach_mode             = PCM
    binding_range           = 0.06
    binding_rate            = 0.2

    ensemble_size           = 1
    k_20                    = 80
    k_01                    = 40
    k_10                    = 2

    stall_force             = 3.85

    display                 = ( color = white; size = 2 )

}
```

```
set hand PCM_CG
{
    hold_growing_end        = 0
    hold_shrinking_end      = 0
    activity                = move
    binding_key             = 2

    detach_mode             = PCM
    binding_range           = 0.12
    binding_rate            = 0.2

    ensemble_size           = 16
    k_20                    = 80
    k_01                    = 40
    k_10                    = 2

    stall_force             = 12.62

    display                 = ( color = white; size = 2 )
}
```